Modelling Laminar Separation Bubbles at Low Reynolds Number

AIAA SciTech Forum
8-12 January 2024, Orlando, FL
AIAA SCITECH 2024 Forum

10.2514/6.2024-1347

Modelling laminar separation bubbles at low Reynolds number

P. Catalano* and D. de Rosa†
CIRA Italian Aerospace Research Center, Capua (CE), 81043, Italy

V. D'Alessandro‡
Dipartimento di Ingengeria Industriale e Scienze Matematche,
Università Politecnica delle Marche, Via Brecce Bianche 12, 60131 Ancona, Italy

A. Marouf§ and Y. Hoarau¶
University of Strasbourg, 4 rue de la Manufacture, 67000 Strasboug, France

M. Miozzi‖
CNR-INM National Research Council- Institute of Marine Engineering, Via di Vallerano 139, 00128 Roma, Italy

M. Righi**
Zurich University of Applied Sciences, Technikumstrasse 9, 8401 Winterthur, Switzerland

Laminar separation bubbles is one of the main critical aspects of flows at low Reynolds number in the range 10^4 – 10^5. The flow separates in the laminar regime and the turbulence developing inside the re-circulation region enhances the momentum transport and the flow can re-attach. Models based on the Reynolds Averaged Navier Stokes equations suffer of two main issues. The determination of the transition onset and the level of the pressure recovery downstream the reattachment of the flow. This paper reports on the activities performed in the framework of a project set-up by a GARTEUR action group. Common test-cases have been performed by several institutions. The low Reynolds number flow around the SD 7003, EPPLER 387, and NACA 0015 airfoils are analyzed. The results are compared to experimental data and large eddy simulations available in literature. The comparison of different methods and models has allowed to individuate advice for the numerical simulation of the laminar separation bubbles.

*Researcher, p.catalano@cira.it, Fluid Mechanics Unit, C.I.R.A.
†Researcher, D.derosa@cira.it, Fluid Mechanics Unit, C.I.R.A.
‡Assistant Professor, v.dalessandro@staff.univpm.it, Dipartimento di Ingengeria Industriale e Scienze Matematche, Marche Polythecnic University
§Assistant Professor, amarouf@unistra.fr, University of Strasbourg, Laboratoire Icube
¶Professor,hoarau@unistra.fr, Head of Mecahnics Department, University of Strasbourg, Laboratoire Icube
‖Researcher, massimo.miozzi@cnr.it, CNR-INM
**Professor, rigm@zhaw.ch, Zurich University of Applied Sciences, Lecturer, righima@ethz.ch, Federal Institute of Technology Zurich, and Visiting Professor at University of Strasbourg, AIAA member

I. Nomenclature

AG	Action Group
c	airfoil chord
C_d	drag coefficient
C_f	skin friction coefficient
C_l	lift coefficient
C_p	pressure coefficient
$GARTEUR$	Group for Aeronautical Research and Technology in EURope
$ILES$	Implicit large eddy simulation
LSB	Laminar separation bubble
LES	Large eddy simulation
M	free-stream Mach number
Q	Second invariant of the velocity-gradient tensor
$RANS$	Reynolds Averaged Navier Stokes
Re	free-stream Reynolds number
SD	Selig-Donovan
SST	Shear Stress Transport
TU_∞	free-stream turbulence intensity
u	Velocity
x	Axial coordinate
y^+	Height of first cell in viscous coordinate
α	Angle of attack
γ	Intermittency function
θ	Momentum thickness

II. Introduction

A laminar separation bubble (LSB) occurs when the flow separates in the laminar regime, and its numerical simulation is still an open point. This phenomenon is the main critical aspect of flows at low Reynolds number, of order of magnitude 10^4-10^5, but is also crucial for flows at high Reynolds numbers. In fact, very tiny laminar separation bubbles are present in airfoil used for turbine applications operating at Reynolds number of the order of magnitude of 10^6.

The action group AG59 of the GARTEUR association (Group for Aeronautical Research and Technology in Europe) has been formed in 2019 to study the numerical/physical modelling of the laminar separation bubbles. The project IMOLA (Improving the MOdelling of LAminar separation bubbles) has been set-up by AG59 members. The focus has been placed on the methods based on the Reynolds Averaged Navier Stokes (RANS) equations. A crucial point in applying the RANS approach is the turbulence modelling. The most critical issues to be addressed are the determination of the transition location and the production of the turbulent kinetic energy. In fact, the presence of a separation bubble means that the separation is laminar and the transition points are very difficult to be set. The turbulence models are instead calibrated for separation in the turbulent flow regime, and need the transition points to be known "a priori". The other critical point is represented by the levels of turbulence inside the recirculation region of the bubble. A proper modelling of the production of the turbulent kinetic energy inside the recirculation region of the bubble should ensure a better reproduction of the pressure recovery and of the bubble length.

Laminar separation bubbles in a wide range of Reynolds numbers (from 10^4 to 10^6) have been analysed in the IMOLA project. Incompressible, but also compressible and transonic flows at low-Reynolds number have been taken into consideration. The interest for the compressible aerodynamics of low-Reynolds number flow has recently grown for the possible use of flying machines for exploring the Martian surface. Laminar instability analysis methods have been also investigated. The focus has been placed on their capability in modelling flow instabilities as they convect through a LSB.

Common test cases have been performed by AG 59 participants and the comparison of the different methods and models has allowed to individuate advices for the numerical simulation of the laminar separation bubbles.

The simulations performed to analyze the laminar separation bubbles at low Reynolds numbers are presented and discussed in this paper. The Selig-Donovan (SD) airfoil at Reynolds number 6.0×10^4, the Eppler 387 airfoil at Reynolds number 2.0×10^5, and the NACA 0015 airfoil at Reynolds number 1.8×10^5 are the test-cases that have been considered. The AG59 members involved in the activities reported in this paper are the Italian Aerospace Research Center (CIRA), the Institute of Marine Engineering of National Research Council of Italy (CNR-INM), the Marche Polytechnic University (UNIVPM), and University of Strasbourg (UNISTRA).

III. Numerical and experimental methods

The numerical methods and models used by AG59 members for the simulation of laminar separation bubbles at low Reynolds number are described in this section.

A. CIRA

The interest of CIRA in the project IMOLA has been in the development and assessment of a methodology for low-Reynolds number flows.

A $\kappa - \omega$ SST transition model based on the intermittency function γ [1] has been recently implemented in the in-house developed code UZEN [2, 3]. This model can be particularly suited for the simulation of the laminar separation bubbles since it allows for simulations without an *a priori* knowledge of the transition location.

Catalano and de Rosa applied the γ model to laminar separation bubbles [4]. The bubble is found with a good estimation of the length, but the minimum of the C_f and the pressure recovery in the reattachment region are underestimated. This issue was addressed by Bernardos *et al.* [5] that proposed the LSST $\kappa - \omega$ model. This is based on a function f_{tr} that boosted the production of the turbulent kinetic energy κ inside the bubble. Excellent results were achieved. However, the model was coupled to the the AHD–Gleyzes transition prediction criterion, since the function f_{tr} requires the "a priori" knowledge of the separation and transition points.

1. New proposed Model

The Menter's intermittency function at the wall γ_w and the Bernardos' transition function f_{tr} are shown in figure 1. Actually, the two functions exhibit a similar qualitative behaviour. The physical phenomena simulated by the two

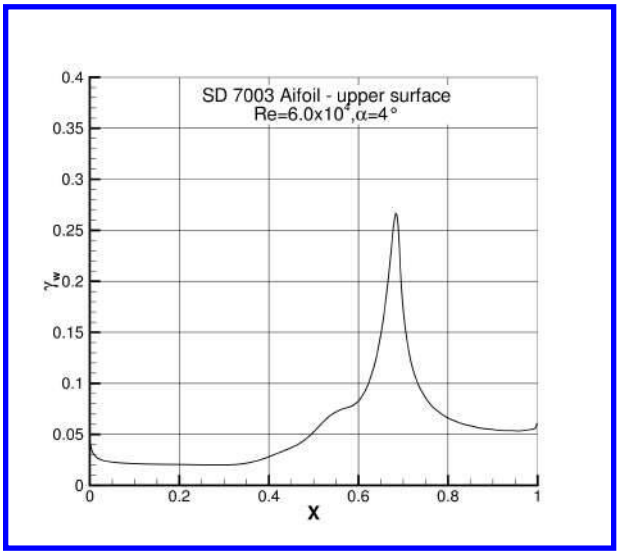

(a) Intermittency function γ at the wall (SD 7003 airfoil $Re = 6.0 \times 10^4$, $\alpha = 4°$)

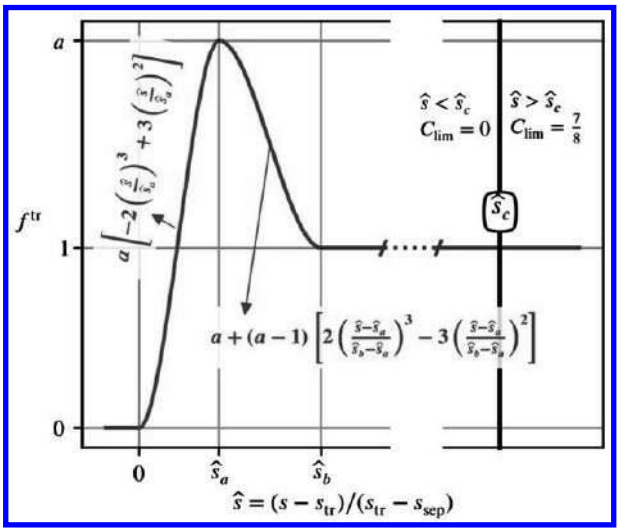

(b) Function f_{tr} [5]

Fig. 1 Intermittency function γ_w and f_{tr} function [5]

functions must be correlated, with the difference that γ_w is an order of magnitude smaller than f_{tr}, thus leading to an

insufficient production of turbulence. The basic idea of the developed model has been to amplify Menter's intermittency function in order to fit the values of f_{tr} at the wall. The purpose is twofold. Taking advantage of the γ function for information on the transition, and of the capability of the Bernardos' transition function f_{tr} in boosting the production of turbulence in the rear part of the bubble.

Determination of a fitting function Simulations have been performed by the Menter SST $\kappa - \omega - \gamma$ [1] model. The flow around the SD7003 airfoil at Reynolds number 6.0×10^4, the Eppler 387 airfoil at Reynolds number 3.0×10^5, and the NACA 0015 airfoil at Reynolds number 1.8×10^5 have been considered. A C topology grids with 1328×192 cells for the EPPLER 387 and NACA 0015 and 1512×192 cells for the SD 7003 airfoil have been employed. It has been verified that the values of y^+ are under one for all the three airfoils.

The intermittency function at the wall γ_w has been computed for each bubble, as well as the separation, transition and reattachment locations. An interesting correlation has been found between transition and reattachment locations and the γ_w function. The transition occurs when the first derivative of the intermittency function $\gamma_w^{'}$, reaches a local maximum value. The reattachment occurs near the location where $\gamma_w^{'}$ has his absolute minimum value. No correlation has been found for the separation location. The intermittency function has a constant behaviour where the flow separation occurs. This correlation has been verified for all the simulations performed.

A fitting function F_{fit}, that permits to recover f_{tr} from γ_w, has been determined in a four-step approach :

1) the Bernardos' transition function f_{tr} has been computed by the results of the simulations with Menter $\kappa - \omega - \gamma$ model;
2) a fitting of the intermittency function at the wall γ_w with Bernardos' transition function was performed for each LSB computed;
3) a mean fitting function was determined for each airfoil and interpolated with a parabola;
4) the final F_{fit} was determined as the mean parabola between the three parabolas obtained for the three airfoil (figure 2).

The F_{fit} is described by the following equation: $z = a\,\bar{x}^2 + b\,\bar{x} + c$, where a translation is performed through $\bar{x} = x - x_0$, to make the first zero of the parabola coincident with the transition point x_{tr}. The coefficients of the

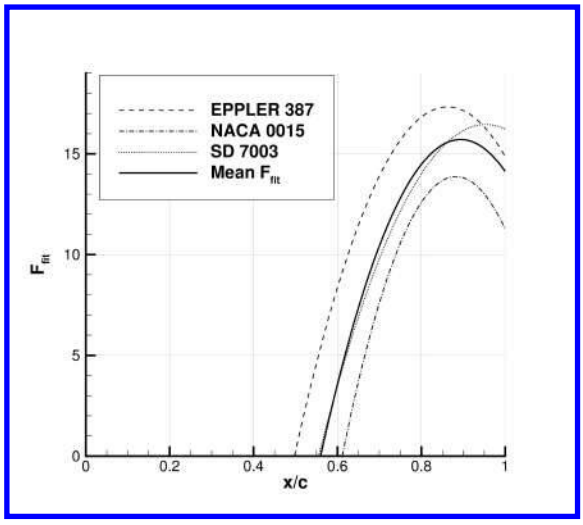

Fig. 2 Mean interpolating parabola of the fitting functions.

parabola are reported in table 1.

a	b	c
-140.8227	251.6973	-96.7556

Table 1 Coefficients for the fitting function.

The proposed model [6] is a merging of the two models. The basis is the Menter $\kappa - \omega$ SST turbulence model coupled with γ transition model, with the modification of the production terms for κ and ω, that are now multiplied by the fitting function $F_{fit}(x, x_{tr})$.

$$\begin{aligned}\frac{\partial(\rho\kappa)}{\partial t} + \frac{\partial(\rho\kappa u_j)}{\partial x_j} &= \gamma\, F_{fit}\, P_k - P_k^{lim} - max(\gamma, 0.1)\cdot D_k \\ &+ \frac{\partial}{\partial x_j}\left[(\mu + \sigma_k \mu_t)\frac{\partial \kappa}{\partial x_j}\right] \end{aligned} \tag{1}$$

$$\frac{\partial(\rho\omega)}{\partial t} + \frac{\partial(\rho\omega u_j)}{\partial x_j} = \gamma\, F_{fit}\, \frac{\omega}{\kappa}\tau_{ij}\frac{\partial u_i}{\partial x_j} - \beta\rho\omega^2 + \frac{\partial}{\partial x_j}\left[(\mu + \sigma_\omega \mu_t)\frac{\partial \omega}{\partial x_j}\right] + 2(1 - F_1)\rho\sigma_{\omega_2}\frac{1}{\omega}\frac{\partial \kappa}{\partial x_j}\frac{\partial \omega}{\partial x_j} \tag{2}$$

$$\frac{\partial(\rho\gamma)}{\partial t} + \frac{\partial(\rho\gamma u_j)}{\partial x_j} = P_\gamma - E_\gamma + \frac{\partial}{\partial x_j}\left[(\mu + \frac{\mu_t}{\sigma_\gamma})\frac{\partial \omega}{\partial x_j}\right] \tag{3}$$

The fitting function has the role of enhancing the turbulence production in the bubble zone, just as Bernardos' transition function. The $F_{fit}(x, x_{tr})$ is dependent on the transition location with x_{tr} retrieved by the derivative of intermittency function at the wall $\gamma_w^{'}$.

B. Marche Politechnic University

The interest of UNIVPM research team has been to investigate the effectiveness of Spalart-Allmaras turbulence model coupled with local correlation based (LCTM) transition models. Specifically, two different approaches, consisting in the adoption of one or two equations for transition modeling, have been considered. The equation of the Spalart-Allmaras model is written as

$$\frac{\partial \tilde{\nu}}{\partial t} + \frac{\partial}{\partial u_j}\left(u_j \tilde{\nu}\right) - \mathrm{P}_{\tilde{\nu}} + \mathrm{D}_{\tilde{\nu}} - \frac{c_{b2}}{\sigma}\frac{\partial \tilde{\nu}}{\partial x_j}\frac{\partial \tilde{\nu}}{\partial x_j} - \frac{1}{\sigma}\frac{\partial}{\partial x_j}\left[(\nu + \tilde{\nu})\frac{\partial \tilde{\nu}}{\partial x_j}\right] = 0, \tag{4}$$

with the turbulent viscosity, ν_t computed according to the $\tilde{\nu}$ variable as

$$\nu_t = f_{v1}\tilde{\nu}, \tag{5}$$

1. γ–$\widetilde{\mathrm{Re}}_{\theta,t}$–SA transition model

In this approach, two transport equations for the intermittency function γ and the transition momentum thickness Reynolds number $\widetilde{\mathrm{Re}}_{\theta,t}$ are used to model the transition:

$$\begin{aligned}&\frac{\partial \gamma}{\partial t} + \frac{\partial}{\partial x_j}\left(u_j \gamma\right) = \mathrm{P}_\gamma - \mathrm{D}_\gamma + \frac{\partial}{\partial x_j}\left[\left(\nu + \frac{\nu_t}{\sigma_f}\right)\frac{\partial \gamma}{\partial x_j}\right], \\ &\frac{\partial \widetilde{\mathrm{Re}}_{\theta,t}}{\partial t} + \left(u_j \widetilde{\mathrm{Re}}_{\theta,t}\right) = \mathrm{P}_{\theta,t} + \frac{\partial}{\partial x_j}\left[\sigma_{\theta,t}\left(\nu + \nu_t\right)\frac{\partial \widetilde{\mathrm{Re}}_{\theta,t}}{\partial x_j}\right].\end{aligned} \tag{6}$$

The source terms in the γ equation are defined as:

$$\begin{aligned}&\mathrm{P}_\gamma = c_{a1} S \left[\gamma \mathrm{F}_{\mathrm{onset}}\right]^{0.5}\left(1 - c_{e1}\gamma\right)\mathrm{F}_{\mathrm{length}}, \\ &\mathrm{D}_\gamma = c_{a2}\Omega\gamma\mathrm{F}_{\mathrm{turb}}\left(c_{e2}\gamma - 1\right),\end{aligned} \tag{7}$$

The term $\mathrm{F}_{\mathrm{onset}}$ in P_γ is computed as:

$$\mathrm{F}_{\mathrm{onset}} = \max\left(\mathrm{F}_{\mathrm{onset},2} - \mathrm{F}_{\mathrm{onset},3}, 0\right) \tag{8}$$

with

$$\begin{aligned}&\mathrm{F}_{\mathrm{onset},2} = \min\left(\max\left(\mathrm{F}_{\mathrm{onset},1}, {\mathrm{F}_{\mathrm{onset},1}}^4\right), 4\right), \\ &\mathrm{F}_{\mathrm{onset},3} = \max\left(2 - \left(\frac{\mathrm{R_T}}{2.5}\right)^3, 0\right), \\ &\mathrm{F}_{\mathrm{onset},1} = \frac{\mathrm{Re}_\nu}{2.193\mathrm{Re}_{\theta,c}}.\end{aligned} \tag{9}$$

where $\mathrm{Re}_{\theta,c}$ represent the critical Reynolds number where the intermittency function starts to increase. In eq. 9 the terms Re_ν and $\mathrm{R_T}$ are obtained as follows

$$\mathrm{Re}_\nu = \frac{Sd^2}{\nu}, \qquad \mathrm{R_T} = \frac{\nu_t}{\nu}. \tag{10}$$

and the coefficient $\mathrm{F_{turb}}$ in D_γ is defined as:

$$\mathrm{F_{turb}} = \exp\left(-\frac{\mathrm{R_T}}{4}\right)^4. \tag{11}$$

The following equation is adopted for the source term $\mathrm{P}_{\theta,t}$ of the transport equation for $\widetilde{\mathrm{Re}}_{\theta,t}$

$$\mathrm{P}_{\theta,t} = \frac{c_{\theta,t}}{\mathrm{T}}\left(\mathrm{Re}_{\theta,t} - \widetilde{\mathrm{Re}}_{\theta,t}\right)\left(1 - \mathrm{F}_{\theta,t}\right). \tag{12}$$

In eq. 12 the last term $\mathrm{F}_{\theta,t}$ is defined as:

$$\mathrm{F}_{\theta,t} = \min\left(\max\left(\exp\left(-\frac{u_j u_j}{375\Omega\nu\widetilde{\mathrm{Re}}_{\theta,t}}\right)^4, 1 - \left(\frac{\gamma - 1/c_{e2}}{1 - 1/c_{e2}}\right)^2\right), 1.0\right). \tag{13}$$

The term T which appears in $\mathrm{P}_{\theta,t}$ is defined as $500\nu/|\mathbf{u}|^2$. The following closure constants are adopted for the transition model,:

$$c_{a1} = 2.0, \quad c_{a2} = 0.06, \quad c_{e1} = 1.0, \tag{14}$$

$$c_{e2} = 50, \quad c_{\theta,t} = 0.03, \quad \sigma_f = 1.0, \tag{15}$$

$$\sigma_{\theta,t} = 2.0. \tag{16}$$

Empirical correlations in the model

Like other γ–$\widetilde{\mathrm{Re}}_{\theta,t}$ approaches available in the literature, the present model contains three empirical correlations needed to compute $\mathrm{Re}_{\theta,t}$, $\mathrm{Re}_{\theta,c}$ and $\mathrm{F_{length}}$.
The correlation developed by Menter et al. [7] for $\mathrm{Re}_{\theta,t}$ is adopted:

$$\mathrm{Re}_{\theta,t} = \begin{cases} \left(1173.51 - 589.428 \cdot Tu + 0.2196/Tu^2\right) F\left(\lambda_\theta\right) & Tu \le 1.3 \\ 331.5\left(Tu - 0.5668\right)^{-0.671} F\left(\lambda_\theta\right) & Tu > 1.3 \end{cases}, \tag{17}$$

$$F\left(\lambda_\theta\right) = \begin{cases} 1 + \left[12.986\lambda_\theta + 123.66\lambda_\theta^2 + 405.689\lambda_\theta^3\right]\exp\left(-\left(\frac{Tu}{1.5}\right)^{1.5}\right) & \lambda_\theta \le 0 \\ 1 + 0.275\left[1 - \exp\left(-35\lambda_\theta\right)\right]\exp\left(-\frac{Tu}{0.5}\right) & \lambda_\theta > 0 \end{cases}. \tag{18}$$

It is important to note that the correlations in eq. 17, 18 contain the turbulence intensity Tu. In the framework of the k–ω model, Tu can be computed using the solution to k equation. The approach introduced in [8] has been employed. Specifically, $Tu = Tu_\infty$ is set for all the points of the flow field.
Moreover $\mathrm{Re}_{\theta,t}$ is computed by iterating on the value of θ_t, since $\mathrm{Re}_{\theta,t}$ is a function of θ_t itself because of the presence of λ_θ. Differently, the correlations introduced by Malan et al. [9] for $\mathrm{Re}_{\theta,c}$ and $\mathrm{F_{length}}$ are used:

$$\mathrm{Re}_{\theta,c} = \min\left(0.615\widetilde{\mathrm{Re}}_{\theta,t} + 61.5, \widetilde{\mathrm{Re}}_{\theta,t}\right), \tag{19}$$

$$\mathrm{F_{length}} = \min\left(\exp\left(7.168 - 0.01173\widetilde{\mathrm{Re}}_{\theta,t}\right) + 0.5, 300\right). \tag{20}$$

$\tilde{\nu}$ equation coupling with γ–$\widetilde{\mathrm{Re}}_{\theta,t}$ model

The production and destruction terms that appear in the $\tilde{\nu}$ transport equation are suitably defined as follows:

$$\begin{aligned} \mathrm{P}_{\tilde{\nu}} &= \gamma_{\mathrm{eff}} c_{b1} \tilde{S} \tilde{\nu}, \\ \mathrm{D}_{\tilde{\nu}} &= c_{w1} f_w \left(\frac{\tilde{\nu}}{d}\right)^2. \end{aligned} \tag{21}$$

The term γ_{eff} in eq. 21 is devoted to model the separation-induced transition and it is defined as follows:

$$\gamma_{\mathrm{eff}} = \max\left(\gamma, \gamma_{\mathrm{sep}}\right) \tag{22}$$

with

$$\gamma_{\mathrm{sep}} = \min\left(2.0 \cdot \max\left[0, \left(\frac{\mathrm{Re}_{\nu}}{3.235\mathrm{Re}_{\theta,c}}\right) - 1\right] \mathrm{F}_{reattach}, 2.0\right) \mathrm{F}_{\theta,t} \tag{23}$$

and

$$\mathrm{F}_{reattach} = \exp\left(-\frac{\mathrm{R_T}}{20}\right)^4. \tag{24}$$

2. γ–$\widetilde{\mathrm{Re}}_{\theta,t}$–SA20 transition model

This version of the γ–$\widetilde{\mathrm{Re}}_{\theta,t}$ transition model exactly replicates the framework above described. The only difference, compared to the γ–$\widetilde{\mathrm{Re}}_{\theta,t}$–SA model, is the c_{w2} coefficient which controls the strength of the near–wall destruction term in $\tilde{\nu}$ equation, [10]. In this case, c_{w2} is replaced by the function

$$c_{w2LRe} = c_{w4} + \frac{c_{w5}}{\left(\frac{\chi}{40} + 1\right)^2} \tag{25}$$

with $c_{w4} = 0.21$ and $c_{w4} = 1.5$.

This approach was presented by Spalart and Garbaruk, [11], to reduce destruction term in the SA equation in the near–wall region to increase the skin friction.

3. $\log\gamma$–SA transition model

A second strategy to include transitional effects into the Spalart–Allmaras turbulence model has been considered. Specifically, one equation for $\tilde{\gamma} = \log\gamma$ is solved to model laminar–to–turbulent transition. This method, formerly introduced by Ilinca and Pelletier, [12], is very attractive because it allows guaranteeing the positivity of the intermittency function. Moreover the logarithmic distribution of a variable ensures a much smoother behaviour with the respect to the use of the primitive variable itself. This is a focal point, because the baseline model formulation exhibits blow–up of the computations.

The transport equation for $\tilde{\gamma}$ is obtained by changing $\gamma = \exp(\tilde{\gamma})$ in the intermittency equation reported in Liu et al. [13]:

$$\frac{\partial\tilde{\gamma}}{\partial t} + \frac{\partial}{\partial x_j}\left(u_j\tilde{\gamma}\right) = \mathrm{P}_{\tilde{\gamma}} - \mathrm{D}_{\tilde{\gamma}} + \frac{\partial}{\partial x_j}\left[\left(\nu + \nu_t\right)\frac{\partial\tilde{\gamma}}{\partial x_j}\right] + \left(\nu + \nu_t\right)\frac{\partial\tilde{\gamma}}{\partial x_j}\frac{\partial\tilde{\gamma}}{\partial x_j}. \tag{26}$$

Production and destruction terms for $\tilde{\gamma}$ equation have the following expressions:

$$\mathrm{P}_{\tilde{\gamma}} = \mathrm{F}_{\mathrm{length}} S\left(1 - e^{\tilde{\gamma}}\right)\mathrm{F}_{\mathrm{onset}} \qquad \mathrm{D}_{\tilde{\gamma}} = c_{a2}\Omega\mathrm{F}_{\mathrm{turb}}\left(c_{e2}e^{\tilde{\gamma}} - 1\right)\mathrm{F}_{\mathrm{onset}}. \tag{27}$$

$\mathrm{F}_{\mathrm{onset}}$ term in eq. 27 is defined as in the γ–$\widetilde{\mathrm{Re}}_{\theta,t}$ framework. Differently, $\mathrm{F}_{\mathrm{onset},2}$ and $\mathrm{F}_{\mathrm{onset},3}$ are re–calculated as follows:

$$\begin{aligned} \mathrm{F}_{\mathrm{onset},2} &= \min\left(\mathrm{F}_{\mathrm{onset},1}, 2.0\right), \\ \mathrm{F}_{\mathrm{onset},3} &= \max\left(1 - \left(\frac{\mathrm{R_T}}{3.5}\right)^3, 0\right). \end{aligned} \tag{28}$$

The following relation in adopted for $\mathrm{F}_{\mathrm{turb}}$ in this LCTM model:

$$\mathrm{F}_{\mathrm{turb}} = \exp\left(-\frac{\mathrm{R_T}}{2}\right)^4. \tag{29}$$

It is worth to remark that the constants c_{a2} and c_{e2} assume the same values reported in eq. 14.
The parameter F_{length} is fixed at 0.5 as in Lit et al. [13] in order to achieve a smooth growth of the intermittency. On the other hand, $Re_{\theta,c}$ is defined as

$$Re_{\theta,c} = f_{local}\left(Tu_l\right) f_{far}\left(Tu_\infty\right), \tag{30}$$

where

$$\begin{aligned} f_{local}\left(Tu_l\right) &= 803.73\left(Tu_l + 0.6067\right)^{-1.027}, \\ f_{far}\left(Tu_\infty\right) &= -3.162Tu_\infty^2 - 0.4565Tu_\infty + 1.7. \end{aligned} \tag{31}$$

Looking at eqs. 30, 31, it is very easy to note that both the local turbulence intensity and the far–field turbulence information are involved. This is an interesting feature of the log γ–SA correlation based transition model. Indeed, a local turbulence intensity controlling term, f_{local}, is adopted to reflect the effect of local turbulence intensity variation on $Re_{\theta,c}$. The formulation of Cakmakcioglu [14] is used for the local turbulence intensity, Tu_l.
The integration of the log γ model and the Spalart–Allmaras turbulence model is handled using a scheme similar to the γ–$\widetilde{Re}_{\theta,t}$ one. The production term of the modified turbulent viscosity, $P_{\tilde{\nu}}$, is treated exactly as in eq. 21. However, a correlation similar to one suggested by Liu et al. [13] is used for the coefficient γ_{sep}:

$$\gamma_{sep} = \min\left(8.0\max\left[0.0, \left(\frac{Re_\nu}{2Re_{\theta,c}}\right) - 1\right], \gamma_{lim}\right) \tag{32}$$

where γ_{lim} is a user defined parameter imposed equal to 2.5. The same approach proposed by Liu et al. [13] is employed for the destruction term $D_{\tilde{\nu}}$ appearing in turbulence equation:

$$D_{\tilde{\nu}} = \min\left(\max\left(\gamma, 0.5\right), 1.0\right)\left[c_{w1} f_w \left(\frac{\tilde{\nu}}{d}\right)^2\right]. \tag{33}$$

4. Boundary conditions

Boundary conditions for $\tilde{\nu}$ are standard: $\tilde{\nu}_\infty = 3\nu$ at the free stream and $\tilde{\nu} = 0$ at the wall, whereas the boundary condition for γ at the wall is a zero normal gradient. At the inlet, the intermittency is set to 1. The boundary condition for $\widetilde{Re}_{\theta,t}$ at the wall is zero flux; differently, a fixed value condition is adopted at inlet for $\widetilde{Re}_{\theta,t}$. This value is calculated from the specific empirical correlation based on the inlet turbulence intensity.

C. National Research Council - Institute of Marine Engineering

The Institute of Marine Engineering of National Research Council of Italy (CNR-INM) has made available to AG59 members experimental data for the NACA 0015 airfoil at Reynolds number 1.8×10^5. The data include quantitative maps of the friction coefficient at three angles of attack: 3°, 5°, and 10°.

1. Theoretical background

When a fluid flows around an immersed body with slightly different temperature, the body's surface temperature distribution is modified. This modification is quantified by the efficiency in heat exchange of the local flow structures that develop within the (laminar or turbulent) boundary layer. There are at least two approaches to understand the connection between skin friction and temperature distribution on the body's surface. One approach relates the evolution of the temperature distribution to the action of the skin-friction field through the energy equation in its asymptotic form at the wall. The other approach considers the transport of temperature disturbances at the wall as a passive scalar, which unveils the relationship chain connecting the celerity of propagation of thermal blobs with the celerity of propagation of velocity disturbances and eventually with the friction velocity.

The energy equation approach leads to a single-snapshot optical flow-like methodology, called the OF algorithm, which can provide time-resolved, relative skin friction fields. This algorithm requires a temperature field that only originates from the interaction between the colder or warmer fluid and the warmer or colder wall, respectively. Thus, temperature gradients that are not induced by the boundary layer may introduce bias in the skin friction estimation. In contrast, the approach adopted in this analysis considers the transport of the fluctuating component of the temperature field as a passive scalar. Following [15] , Miozzi et al. [16] proposed a physically motivated convection velocity of a passive scalar, which depends on the spectral information in only one direction, either space or time, and on a local

derivative in the remaining direction. In practice, the method consists on minimizing the dissimilarity between the observed behavior and the ideal wave one, conforming to the Taylor hypothesis. In other words, it means finding the characteristic velocity of the reference frame where waves experience the least change if compared to the Taylor hypothesis. This quantity represents the absolute value of the celerity of propagation of the velocity fluctuations. Following the seminal findings of [17], enforced by [15, 18], it is in a linear relationship with the friction velocity u_τ. The proposed method estimates the propagation celerity of temperature fluctuations U_T, and because of its relationship with the friction velocity $\mathbf{u}_\tau$ [19], it estimates the friction coefficient C_f. DLR and CNR-INM cooperated to develop and apply different methodologies to extract skin-friction fields from temperature maps using Temperature Sensitive Paint (TSP) [20]. Sensors relying on this technology yield global temperature data from the whole coated surface, with elevate resolution in space and time [21, 22].

2. Experimental Setup

The experiments were conducted in the CEIMM cavitation tunnel (CNR-INM, Rome, IT), which is a closed-loop water facility with a square test section that has side $B = 600\,\text{mm}$, length $L_S = 2.6\,\text{m}$, and optical access. The nozzle contraction ratio is 5.96 : 1.

The aluminum-made hydrofoil has a symmetric NACA 0015 profile, with a chord length of $C = 120\,\text{mm}$ and a span width equal to the test-section side ($L = B = 600\,\text{mm}$). This corresponds to an aspect ratio and blockage factor of $B/C = 5$ and $C/B = 0.2$, respectively. The model is mounted in the middle of the tunnel transverse side and rotated around its geometric center to set the profile at the investigated angles of attack [23].

The hydrofoil is coated with a TSP functional set of layers. When excited at a wavelength of 405 nm, the TSP emits light at 610 nm with an intensity inversely proportional to the local temperature, undergoing the thermal quenching [21]. The emission is captured by a Photron SA-X fast camera, equipped with Nikkor 50 mm $f/1.4$ optics, holding a long-wave pass filter with a cut-point at 600 nm. The camera captures the emission at a frequency $f_r = 1000\,\text{Hz}$, providing time- and spatially-resolved information about the efficiency of the boundary layer in modifying the temperature statistics distribution. To enhance the signal-to-noise ratio of the thermal fingerprints of the flow structures on the model surface, the body of the hydrofoil is pierced spanwise by three ducts where externally heated water (warmer than the tunnel water) is forced to flow.

The tests reported here investigate the temperature of the hydrofoil's surface at a chord-based Reynolds number $Re = 1.8 \times 10^5$ and Angles of Attack $AoA = [5°,\ 10°]$. At these experimental conditions, the flow uniformity is less than 3% for the vertical component and 1% for the axial one. The components of the freestream turbulence level within the TSP test section, $U' = U_{\text{rms}}/U_\infty$ and $V' = V_{\text{rms}}/U_\infty$, are less than 2% in the central region of the test section, and lower of 1% in the investigated region for the streamwise one.

D. University of Strasbourg

The University of Strasbourg interest during the IMOLA project has been to implement different strategies to improve the numerical simulation of the laminar separation bubble. RANS turbulence models are coupled with additional transport equations to model the correct turbulence development and level in the beginning of the separation and inside the re-circulation regions. The numerical simulations are carried out with the Navier Stokes Multi-Block NSMB solver [24, 25], which includes an ensemble of the most efficient CFD methods, as well as adapted fluid–structure coupling for moving and deformable structures. These developments can be found in [26]. University of Strasbourg has computed real-scale high Reynolds number unsteady turbulent flows thanks to advanced turbulence modelling approaches as improved DDES (Delayed Detached Eddy Simulation) and OES (Organised Eddy Simulation) [27, 28]. These models have proven to be very efficient for simulating critical flow dynamics around 3D wings, to predict separation bubbles and transition locations. Recent studies carried out using NSMB solver and the OES approach captured separation bubbles and the recirculation zones close to the trailing-edge region [29].

1. Description of the NSMB solver

NSMB is being developed in a consortium composed of different universities and industries and is mainly used for aeronautics and aerospace applications over the past 30 years. NSMB has a parallel and a vectorial structure and can run on high-performance computers to solve a wide range of industrial aerodynamics design problems. NSMB solves the Reynolds-averaged Navier Stokes equations for compressible flows on multi-block structured grids. NSMB offers all functionalities of a modern CFD code used for aerospace applications, among others, ALE (Arbitrary

Lagrangian Eulerian) approach [30], turbulence models [26], chemistry modelling, grid flexibility, FSI (Fluid-Structure Interactions) coupling morphing wings modelling and Chimera overlapping technique. Space discretization schemes include 2^{nd}- and 4^{th}-order central schemes with artificial dissipation and various upwind schemes (Roe, AUSM, Van Leer ...) up to 5^{th} order. Time integration methods are explicit (Runge-Kutta schemes) or implicit (LU-SGS) schemes. Convergence acceleration as multigrid, local time stepping, preconditioning, and full multigrid can be used to accelerate the convergence. NSMB also includes a large variety of well-tested and validated turbulence models that are standard in the aeronautical industry, like the one-equation Spalart-Allmaras, [31], the Organized Eddy Simulation model, or the two-equation by Menter [32], that have been applied to the test cases discussed in this paper.

Transition models are implemented in the 1 equation Spalart-Allmaras model and the 2 equation $\kappa - \omega$-SST model as summarized in the following table:

Number of additional equations	Turbulence model
0	Spalart-Allmaras Bas-Cakmakcioglu-Mura [33]
1	γ model of Langtry et. al [1]
2	Original γ-R_θ model of Langtry-Menter [34]

2. DARPA EQUiPS

University of Strasbourg, through a visiting Professor, has also worked on a method based on uncertainty quantification.

Assessing the errors in turbulence modelling is an active research field, as discussed for instance in the review papers [35, 36] and references therein. Several approaches have been put forward over the past few years. For convenience, the DARPA EQUiPS ("Enabling Quantification of Uncertainty in Physics Simulation") module developed for the SU2 CFD suite has been chosen. This module was made available to SU2 users along with a complete tutorial *.

The EQUiPS module focuses specifically on the estimation of uncertainties arising due to turbulence closure models [37]. The rationale behind this approach directly addresses the limitations of classical turbulence models, primarily those associated with the eddy viscosity hypothesis. The methodology is presented in Ref. [36–38] and consists in a comprehensive framework providing effective eigenspace perturbations. This allows directly addressing the anisotropy of the turbulent stress tensor and the turbulent production.

The rationale behind the methodology may also be summarized by stating that eddy-viscosity hypothesis prescribes identical eigenvectors for the modeled Reynolds stress tensor and the mean rate of strain tensor; whereas this is true in simple shear flows, it is not necessarily true in complex engineering flows [39–41].

Within the EQUiPS module, the perturbations added are defined with reference to the barycentric map [42] (figure 3). The EQUiPS module was applied to the transitional SST Langtry-Menter model. Whereas there are no inconsistencies,

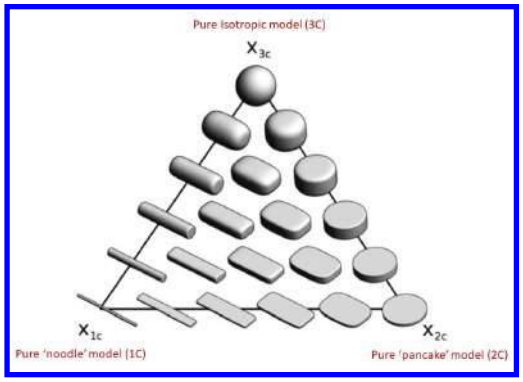

Fig. 3 All possible models (with given a set of eigenvectors) of the Reynolds stress tensor

no other applications are available in the literature. It is also worthwhile mentioning that in the implementation in SU2 the perturbations are introduced via a relaxation factor which cannot be raised above a problem specific threshold.

*https://su2code.github.io/tutorials/UQ_NACA0012/

Five simulations perturbating the Reynolds tensor plus a simulations without any perturbation have been performed for the flow around the SD 7003 airfoil at Re=6.0×10^4 and $\alpha = 4°$. In the figures 4 and 5, the results obtained

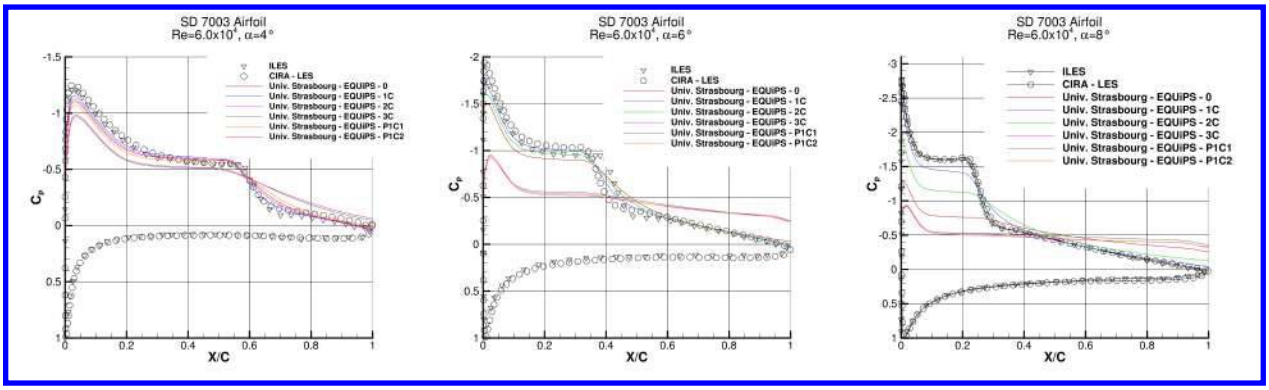

(a) $\alpha = 4°$ (b) $\alpha = 6°$ (c) $\alpha = 8°$

Fig. 4 Skin friction coefficients over the SD7003 airfoil at $Re_\infty = 6.0 \times 10^4$.

without adding any perturbation to the Reynolds stress tensor are indicated with "0". The symbols "1C", "2C" and "3C" concern perturbations of the eigenvalues of the stress tensor, which in practice modify the shape of the Reynolds stress ellipsoid but not its orientation. The symbols "P1C1" and "P1C2" refer to perturbations of the eigenvectors of the stress tensor, which implies modifying the orientation of the Reynolds stress ellipsoid. In particular, "P1C1" aligns the eigenvectors of the Reynolds stress tensor with those of the flow strain rate, besides introducing the eigenvalues perturbation "1C". "P1C2" aligns the eigenvectors of the Reynolds stress tensor with those of the flow strain rate, besides introducing the eigenvalues perturbation "2C". The friction and pressure coefficients obtained by perturbating

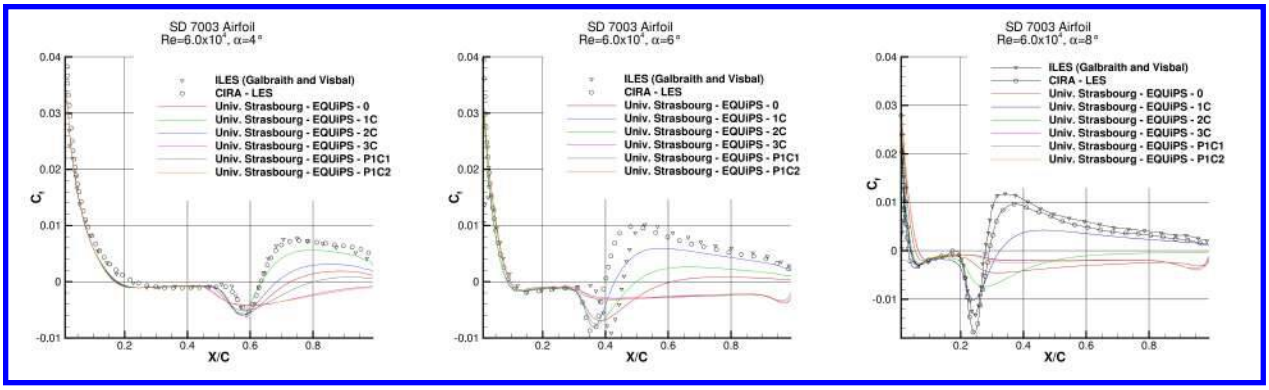

(a) $\alpha = 4°$ (b) $\alpha = 6°$ (c) $\alpha = 8°$

Fig. 5 Skin friction coefficients over the SD7003 airfoil at $Re_\infty = 6.0 \times 10^4$.

the eigenvalue corresponding to the pure "noddle" model "1C" are the closest to the reference LES values.

Unsurprisingly, the results presented for the SD7003 airfoil show large differences between the predictions obtained from the five perturbations of the stress tensor eigenspace. It is worth noting that the perturbation maximising turbulence production leads to the earlier transition.

IV. Results and Discussion

The numerical methods described in the previous sections have been applied to simulate the laminar separation bubbles over three airfoils, the SD 7003 at Reynolds 6.0×10^4, the Eppler 387 at Reynolds 2.0×10^5, and the NACA 0015 at 1.8×10^5 A single block C-topology grid has been used for the three airfoils. A mesh of 768×176 cells for the SD 7003, and about 1300×190 for Eppler 387 and NACA 0015 airfoils have been employed. The height of the first cell in viscous coordinate is shown in figure 6. Good values are obtained for all the airfoils.

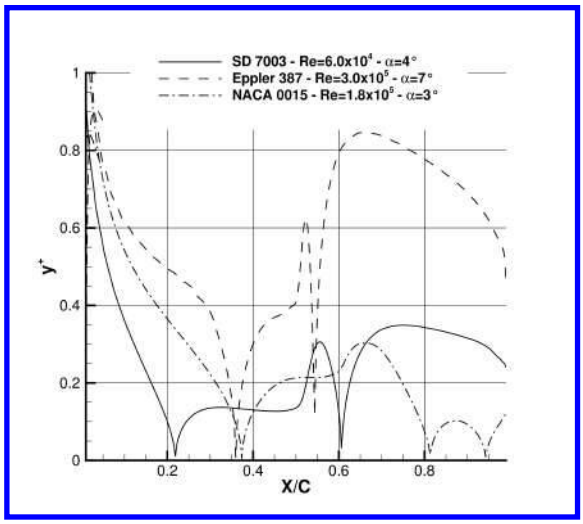

Fig. 6 y^+ for the SD7003, Eppler 387, and NACA0015 airfoils

A. SD 7003 airfoil

The incompressible flow around the Selig-Donovan (SD) 7003 airfoil at Reynolds number of 6.0×10^4 presents very interesting characteristics. A long laminar separation bubble is present on the upper surface of the airfoil that resembles

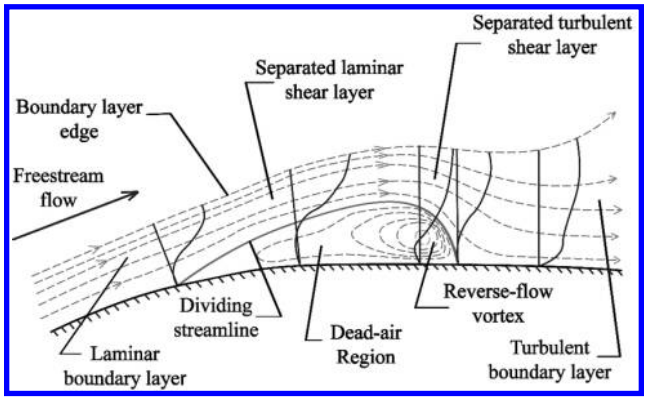

Fig. 7 Structure of a laminar separation bubble

the classical structure of a bubble (figure 7) as reported in literature [43].

Catalano & Tognaccini [44] have performed large eddy simulations of this flow. The evolution of the turbulent structures at $\alpha = 4°$ is presented in figure 8 where the isosurface $Q = -\frac{1}{2}\frac{\partial u_i}{\partial x_j}\frac{\partial u_j}{\partial x_i} = 50$ is shown at different time instants. The iso-surface is coloured by the streamwise velocity in such a way that the region of reverse flow can be discerned. The separation, and the 2D structures forming upstream the transition in the first part of the bubble in the *dead air* region are visible. The development of the turbulence seems to be due to a sort of Kelvin-Helmholtz instability.

The bubble moves upstream as the incidence increases. At high incidence ($\alpha > 10°$), both the separation and the re-attachment point of the bubble do not vary considerably but the recovery of pressure decreases. As α still increases, the flow becomes quite complex and is characterized by a short bubble in the leading edge zone and by a separated region in the central part of the upper surface of the airfoil. Vortices are shed from the laminar separated region in the forward part of the airfoil and flow into the next turbulent separated region. A large vortex is then convected from the airfoil. The stall of the airfoil occurs when the laminar bubble present in the leading edge region and the turbulent separated region join together. All these phenomena can be discerned by the isosurface of Q shown in figure 9 for the flow at $\alpha = 12°$ as reproduced by a large eddy simulation [44, 45].

Pressure and friction coefficients at several incidences are shown in the figures 10 -13. The results have been

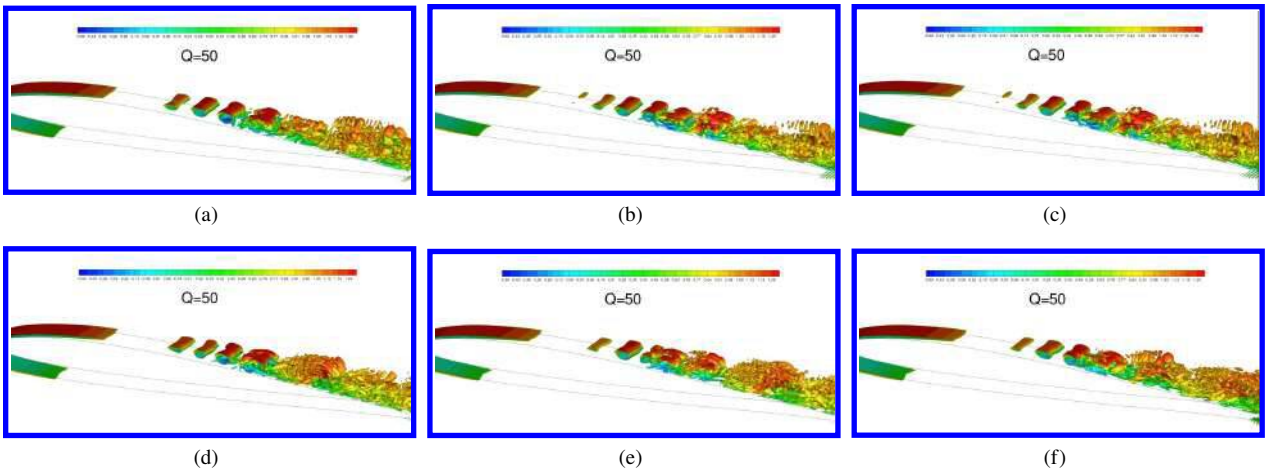

Fig. 8 Laminar separation bubble over the SD 7003 airfoil at Reynolds 6.0×10^4, and $\alpha = 4°$. Isosurface of Q coloured by the streamwise velocity

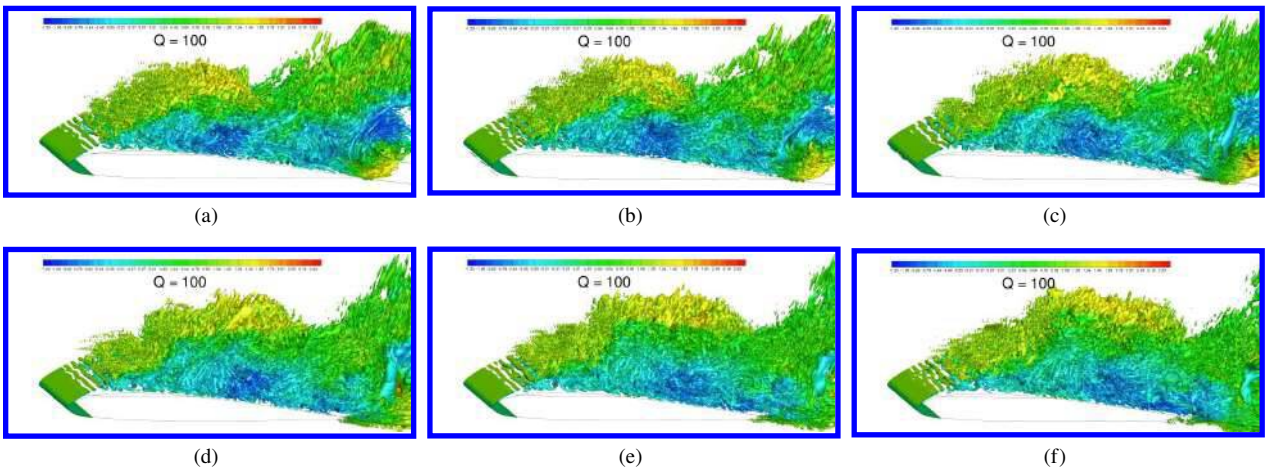

Fig. 9 Laminar separation bubble over the SD 7003 airfoil at Reynolds 6.0×10^4, and $\alpha = 12°$. Isosurface of Q coloured by the streamwise velocity

achieved by CIRA, UNIVPM, and University of Strasbourg by applying several turbulence models and are compared to literature LES data [4, 45–48]. All the turbulence models employ one (γ) or two (γ and Re_θ) equations for modelling the transition. UNIVPM makes use of the Spalart-Allamaras while CIRA and University of Strasbourg of the $\kappa - \omega - \gamma$ SST [34] as "base" model. The results obtained by University of Strasbourg by the EQUiPS model with the "1C" eigenvalue perturbation are also reported.

At $\alpha = 4°$, the two LES data are in very good agreement between them. The model proposed by CIRA (section III.A.1) [6] remarkably improves the results of the $\kappa - \omega - \gamma$ SST model achieving an excellent comparison with LES data for the bubble and for pressure levels. The Spalart Allmaras $\gamma - \widetilde{\mathrm{Re}}_{\theta,t}$-20 (section III.B.2) model provides a good result for pressure coefficient with a slight over-prediciton of the bubble length and an under-prediction of friction levels in the re-attachment region. A good result is also shown by the EQUiPS model.

At $\alpha = 6°$, there is a discrepancy between the LES data mainly in the skin friction coefficient. The CIRA proposed model is in good agreement with the large eddy simulation by CIRA with an overprediciton of the bubble length. The UNIVPM results are also in good agreement with the CIRA LES and present a slight overprediction of the bubble length with and underprediction of the friction levels downstream the bubble. The $\kappa - \omega - \gamma$ model by University of

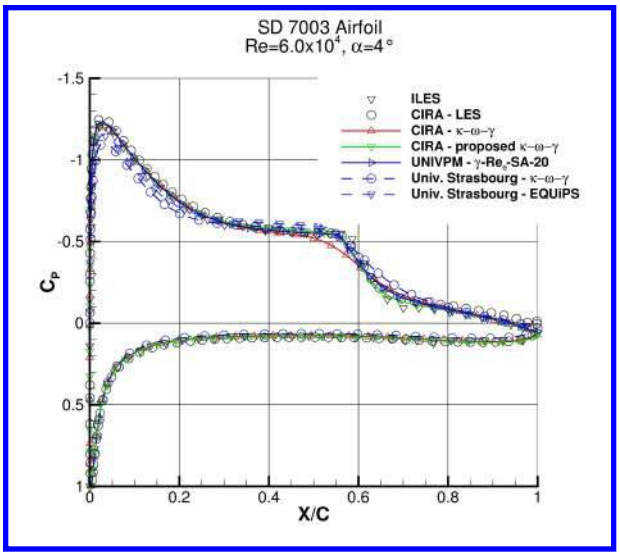

(a) Pressure coefficient

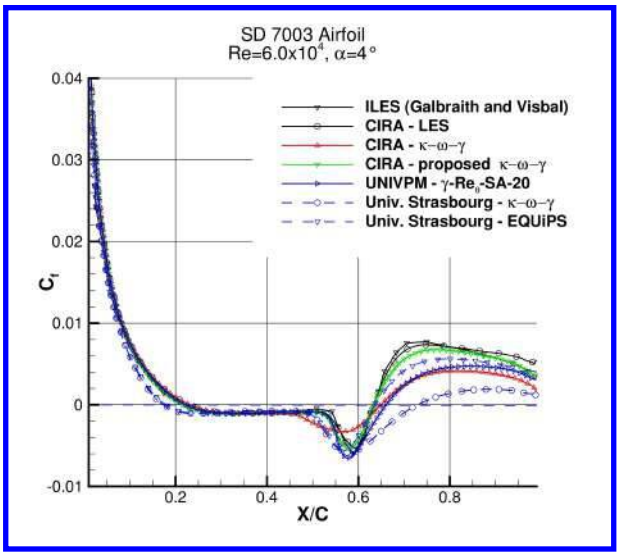

(b) Skin friction coefficient

Fig. 10 Pressure and friction coefficients over the SD7003 airfoil at $\mathrm{Re}_\infty = 6.0 \times 10^4$ and $\alpha = 4°$.

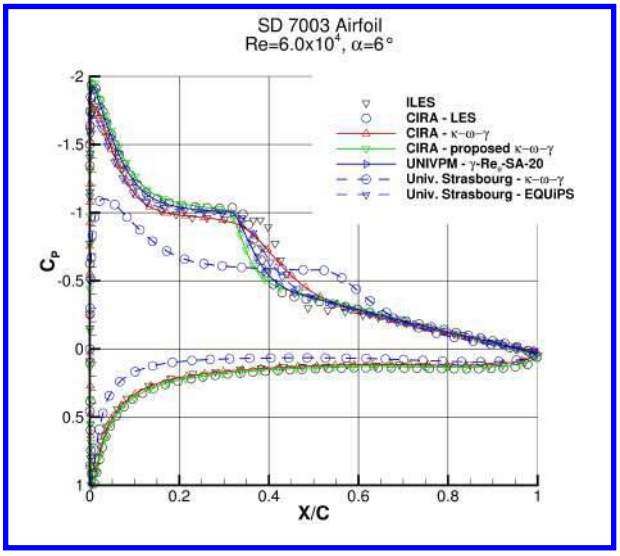

(a) Pressure coefficient

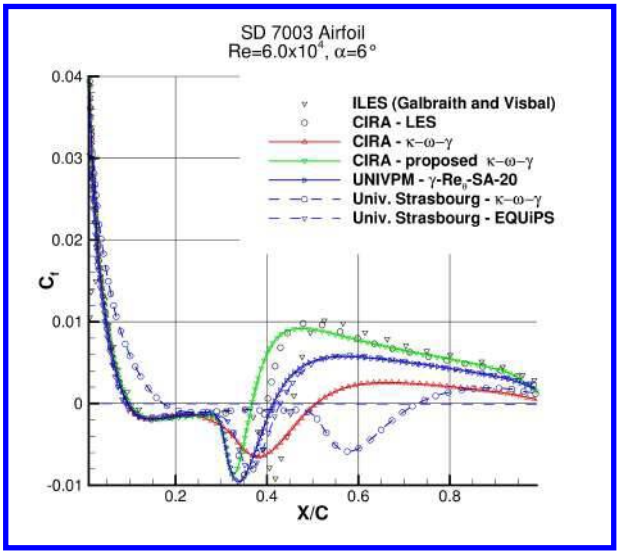

(b) Skin friction coefficient

Fig. 11 Pressure and friction coefficients over the SD7003 airfoil at $\mathrm{Re}_\infty = 6.0 \times 10^4$ and $\alpha = 6°$.

Strasbourg has provided a not converged result while the UQUiPS approach has shown a good result very close to the Spalart Allmaras $\gamma - \widetilde{\mathrm{Re}}_{\theta,t}$-20 model.

At $\alpha = 8°$, the two set of LES data are in very good agreement. The "base" $\kappa - \omega - \gamma$ model shows a very poor convergence. Instead, the CIRA proposed model provides a good result. Both UNIVPM and CIRA data overpredict the pressure level on the upper surface of the airfoil whereas the EQUiPS model provides an underestimation of the C_P. However, a difference between all RANS and LES data is present at this incidence in both C_P and C_f distribution with an underprediciton of the bubble length.

At $\alpha = 10°$ only the RANS data by UNIVPM and the CIRA LES results are available. The incidence is crucial because flow is approaching the stall. The laminar bubble is advanced to the leading-edge region and the pressure

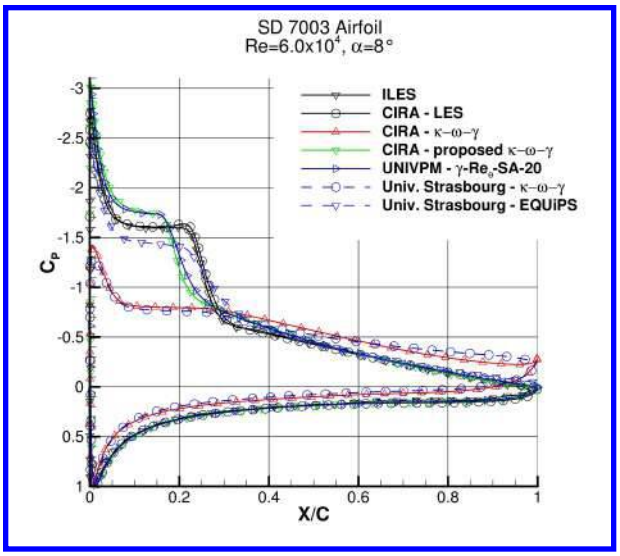

(a) Pressure coefficient

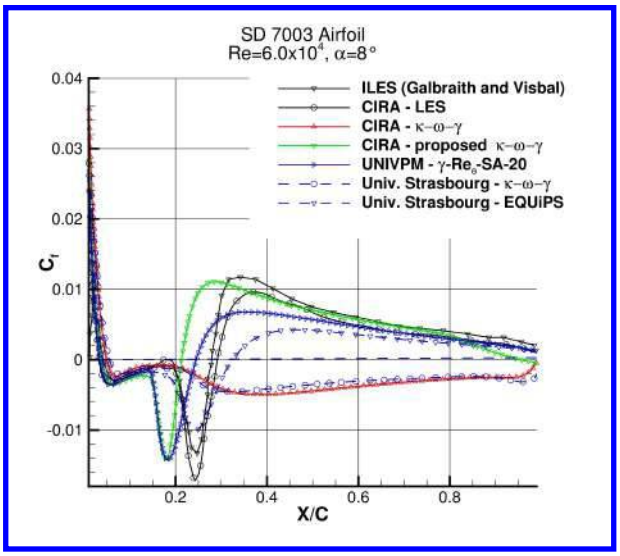

(b) Skin friction coefficient

Fig. 12 Pressure and friction coefficients over the SD7003 airfoil at $Re_\infty = 6.0 \times 10^4$ and $\alpha = 8°$.

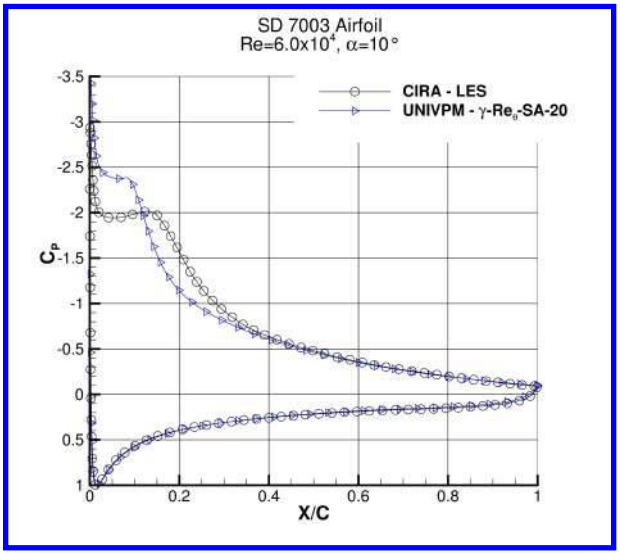

(a) Pressure coefficient

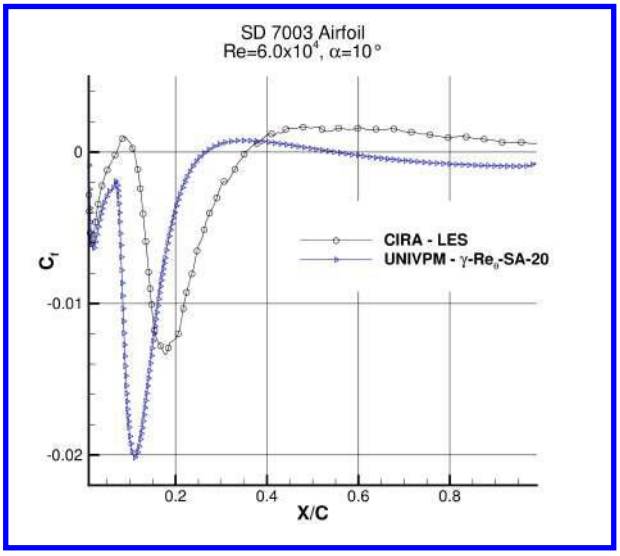

(b) Skin friction coefficient

Fig. 13 Pressure and friction coefficients over the SD7003 airfoil at $Re_\infty = 6.0 \times 10^4$ and $\alpha = 10°$.

recovery downstream the bubble is very weak. The flow is about to separate for LES and is already separated in the RANS results.

Three sets of experimental data are available in literature and have been taken as reference for the aerodynamic coefficients. The measurements from Selig *et al.* at University of Princeton in 1989 [49] and at University of Illinois in 1996 [50] and from Ol *et al.* at Horizontal Free-Surface Wind tunnel (HFWT) at Air Force Research Laboratory in 2005 [30]. The data consists of lift and drag coefficient at several incidences.

The comparison with the numerical data is reported in figure 14 in terms of lift coefficient and drag polar. All the models employed agree well with the experimental data in the linear part of the lift curve. The RANS results by UNIVPM well follow the experiments up to high incidence. The behaviour at the stall is present only in the HFWT data

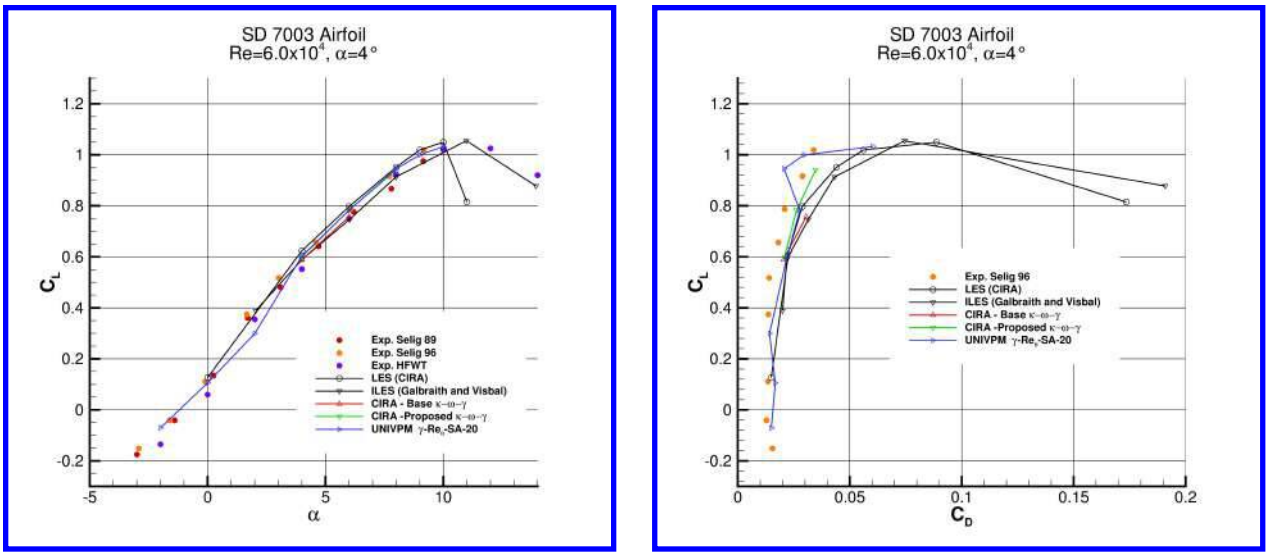

(a) Lift coefficient

(b) Drag polar

Fig. 14 Aerodynamic coefficients over the SD7003 airfoil at $\mathrm{Re}_\infty = 6.0 \times 10^4$.

and is well predicted by the implicit LES. The LES by CIRA, instead, shows an anticipated stall. The RANS results by UNIVPM well follow the experiments up to high incidence.

The numerical data generally present an overprediction of the experimental drag coefficients. available only in Selig 1996 [50]. The UNIVPM data present a sort of laminar "bag" at a lift coefficient around $0.9 - 1.0$.

B. Eppler 387 airfoil

The Eppler 387 airfoil at $\mathrm{Re} = 2 \times 10^5$ has been also studied. The specific case was selected since a large and accurate data set of experimental measurements was published by McGhee et al. [51]. As in the other test cases, different turbulence models have been used. Marche Polytechnic University applied two versions of the Spalart-Allmaras model. Differently, University of Strasbourg used three different transition approaches for both Spalart–Allmaras and k–ω SST turbulence models.

Pressure coefficients obtained are, in general, very consistent with experimental data. This is particularly true for the angles of attack prior to the stall region ($\alpha < 10°$). However, SST $\kappa - \omega$ BCM model was not able to predict transition and the related results seem to more similar to a fully turbulent mode.
A particular mention have to be devoted for $\alpha = 8°$. McGhee et al. observed a LSB near to the leading edge at $\alpha = 8.5°$, while a natural transition in boundary layer was evidenced at $\alpha = 8°$. This behaviour may contribute to explain the discrepancy between the all the numerical and experimental data which can be noted in Fig. 16.

The force coefficients, showed in Fig. 17, confirm the very good consistency between almost all the models adopted and experimental data prior to the stall region. In this case, it is very easy to note as log γ–SA model implementation of Marche Polytechnic University put in evidence the worst behaviour in the stall detection.

C. NACA 0015 airfoil

The NACA 0015 airfoil at $Re = 1.8 \times 10^5$ and $\alpha = 3°$ and $10°$ has been considered. Experimental data [52, 53] and large eddy simulations performed at $\alpha = 3°$, and $10°$ [4] are considered as reference. Different turbulence models have been used. CIRA applied the $\kappa - \omega - \gamma$ in the basic form [34] and the version [6] described in the section III.A.1. Marche Polytechnic University applied two versions of the Spalart-Allmaras model. The flow resulted difficult to be reproduced by the numerical methods, especially at $\alpha = 3°$ with the bubble covering a large portion of the upper surface. This is somehow also confirmed by the experiments, that present a large scatter of the data and a quite complex flow topology at the low incidences [52, 53]. The structure of the bubble, as recovered by a large eddy simulation [4], is

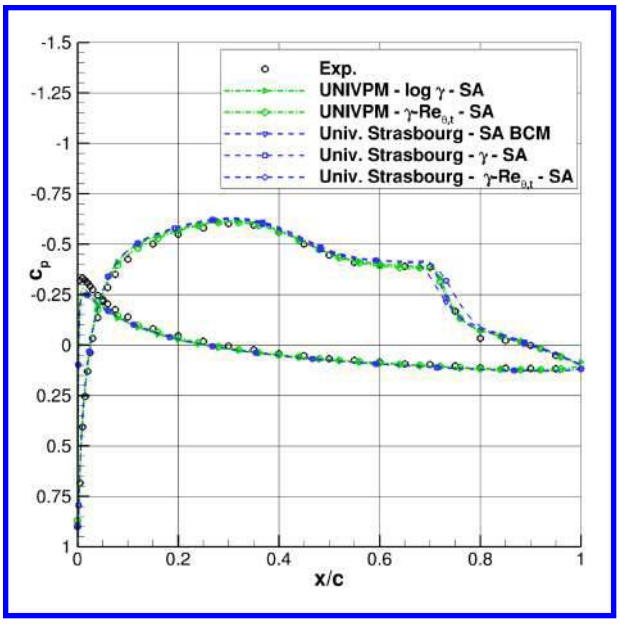

(a) $\alpha = 0°$, SA models.

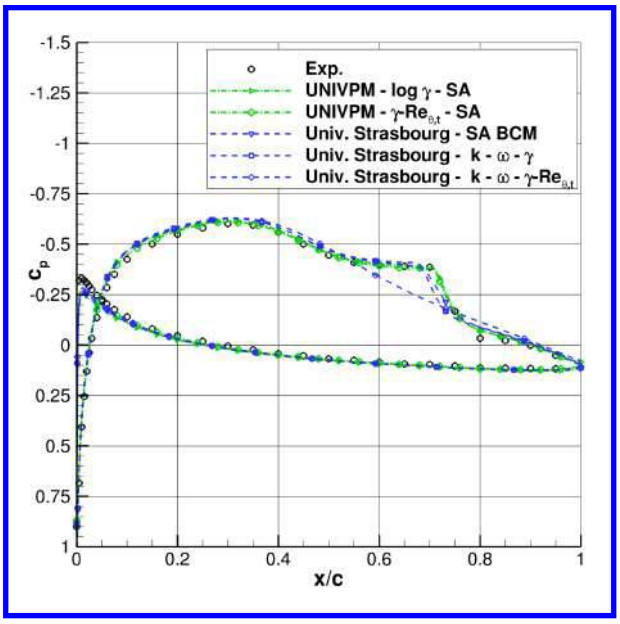

(b) $\alpha = 0°$, SA and k–ω models.

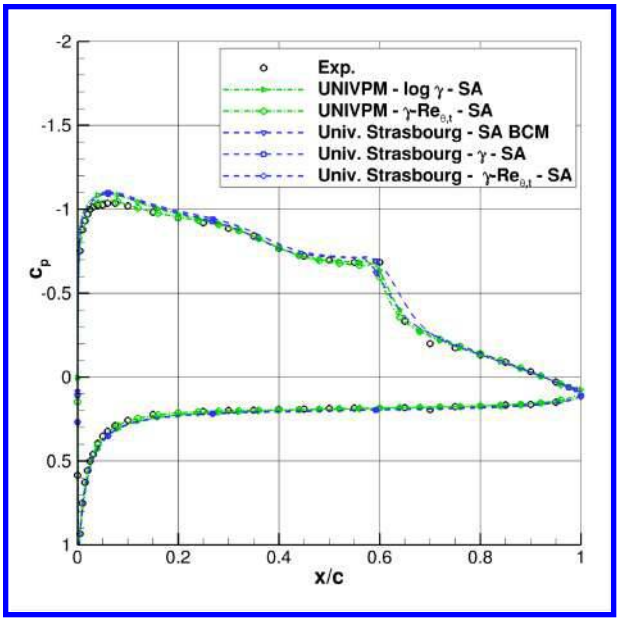

(c) $\alpha = 4°$, SA models.

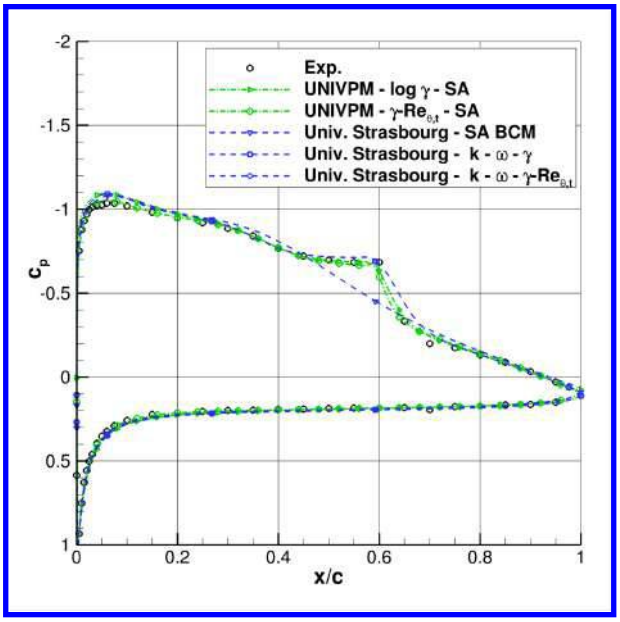

(d) $\alpha = 4°$, SA and k–ω models.

Fig. 15 Pressure coefficients over the E387 airfoil at $Re_\infty = 2 \cdot 10^5$

shown in figure 18 and is similar to the one over the SD7003 airfoil at $\alpha = 4°$.

The data for the flow at $\alpha = 10°$ are reported in the figures 20 and 21. A large eddy simulations [4] is considered for sake of comparison. The time evolution of the turbulent structures [4] is presented in the figure 20. The region of laminar flow with 2D structures is quite restricted, and the flow becomes fully turbulent close to the separation.

The skin friction coefficient is shown in figure 21. The flow presents a laminar bubble in the front part of the airfoil followed by a strong pressure recovery. The flow is close to the separation also in the rear region. The experimental C_f has been extracted from the data, achieved by Temperature Sensitive Paints (TSP), by two unrelated algorithms, and two set of data are reported in figure 21. One is based on the time lag that maximizes the temporal correlation between

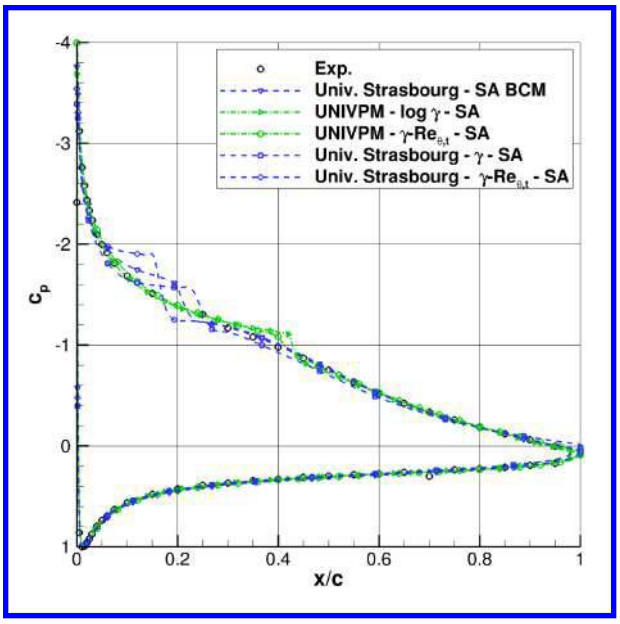

(a) $\alpha = 8°$, SA models.

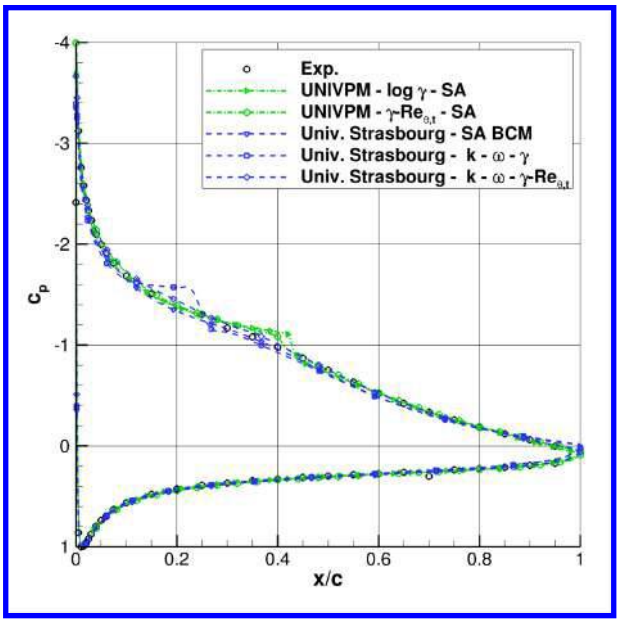

(b) $\alpha = 8°$, SA and k–ω models.

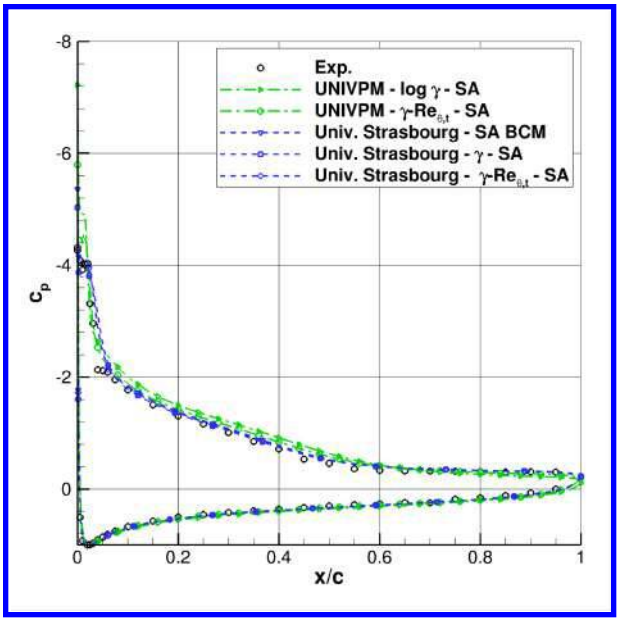

(c) $\alpha = 12°$, SA models.

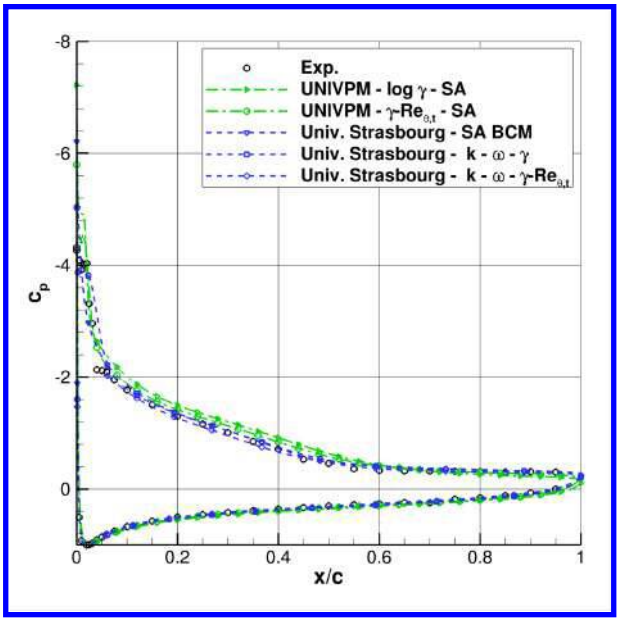

(d) $\alpha = 12°$, SA and k–ω models.

Fig. 16 Pressure coefficients over the E387 airfoil at $Re_\infty = 2 \cdot 10^5$

stream-wise aligned points; the other is based on an optical flow analogy obtained from the asymptotic expansion of the energy equation at the wall [54]. The C_f obtained by the temporal correlation is the one that better agrees with the LES results. The $\kappa - \omega - \gamma$ model proposed by CIRA and the Spalart-Allmaras γ–$\widetilde{\mathrm{Re}}_{\theta,t}$–SA20 transition model by UNIVPM provide results in good agreement with both LES and experimental data. The separation and the reattachment points are slightly shifted, and the pressure recovery is fairly good. A separated region in the trailing-edge zone is present in the CIRA RANS results.

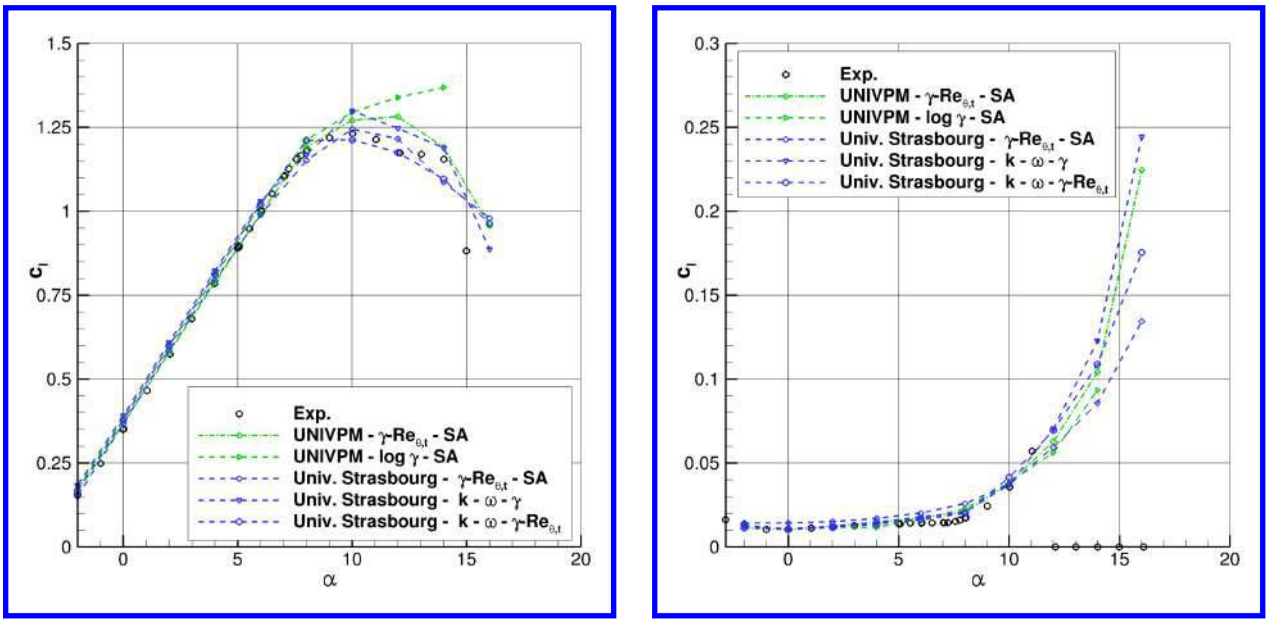

(a) $c_l-\alpha$ (b) $c_d-\alpha$

Fig. 17 the E387 airfoil at $Re_\infty = 2 \cdot 10^5$, forces coefficients.

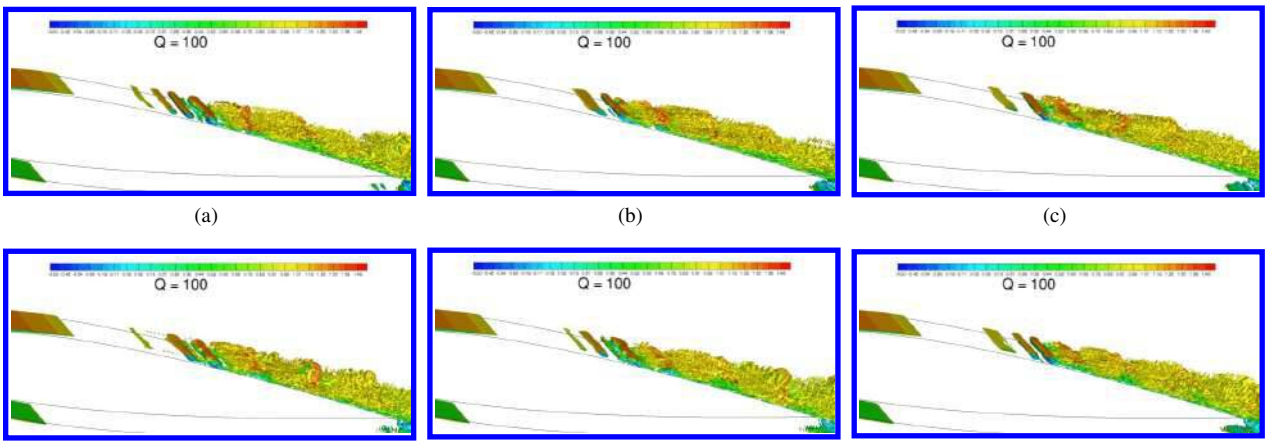

(a) (b) (c)

(d) (e) (f)

Fig. 18 Laminar separation bubble over the NACA 0015 airfoil at Reynolds 1.8×10^5, and $\alpha = 3°$. Isosurface of Q coloured by streamwise velocity

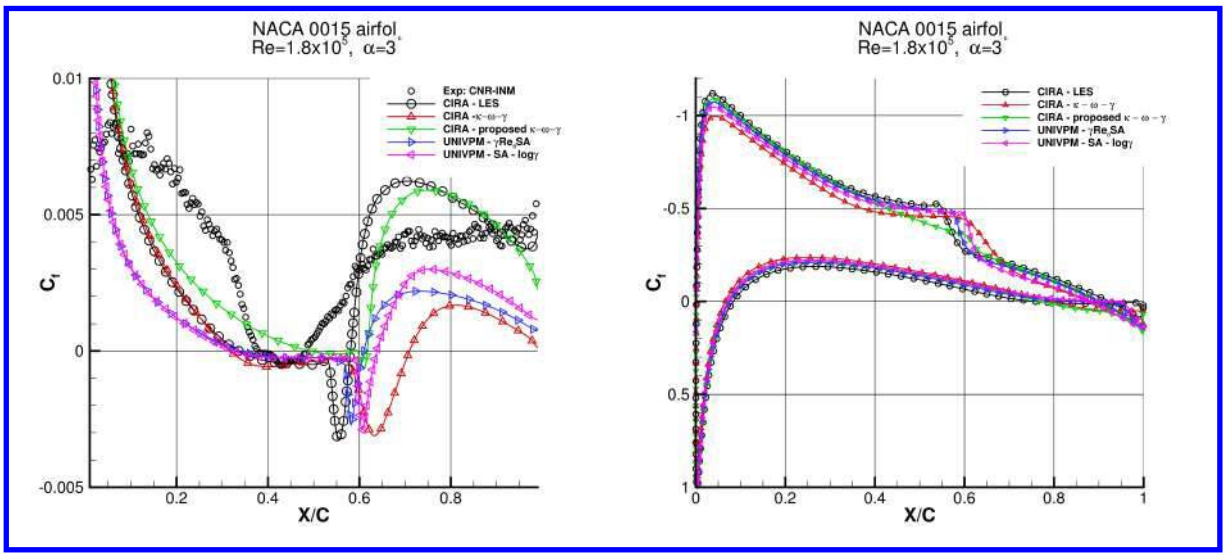

(a) Skin friction coefficient

Fig. 19 Pressure and friction coefficients over the NACA 0015 airfoil at $Re_\infty = 1.8 \times 10^5$ and $\alpha = 3°$.

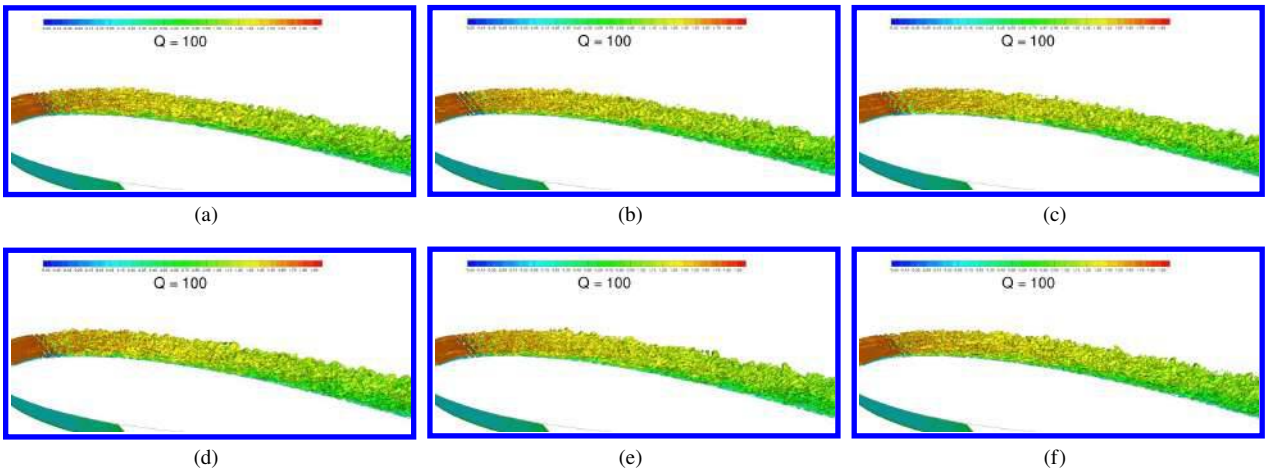

(a) (b) (c)

(d) (e) (f)

Fig. 20 Laminar separation bubble over the NACA 0015 airfoil at Reynolds 1.8×10^5, and $\alpha = 10°$. Isosurface of Q coloured by streamwise velocity

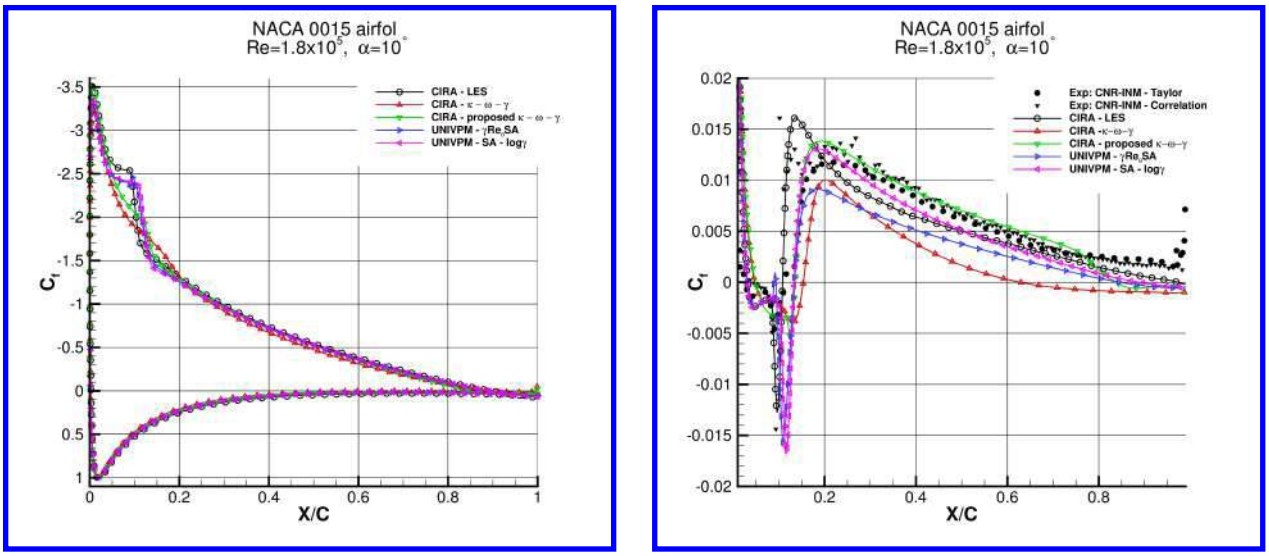

(a) Pressure coefficient

(b) Skin friction coefficient

Fig. 21 Pressure and friction coefficients over the NACA 0015 airfoil at $Re_\infty = 1.8 \times 10^5$ and $\alpha = 10°$.

V. Conclusions

The action group 59 of the GARTEUR association started its activities in February 2019 with the main aim of improving the numerical modelling of laminar separation bubbles. The focus has been placed on RANS methods and turbulence modelling. Several test cases covering laminar separation bubbles at low and high Reynolds numbers and also in the compressible flow regime have been considered. This paper has reported on the activities performed for the laminar separation bubbles at low Reynolds number.

Some best practice advices can be summarized. The importance of employing turbulence models making use of transition functions (γ, and/or Re_θ) has been highlighted. Good results have been achieved by employing the Spalart-Allmaras model with transition functions, especially the version modified for decreasing the destruction term of the model. This has as a consequence the increase of the skin friction levels in the recovery region of the flow. The same effect can be obtained by a function that multiplies the production term of the kinetic turbulence equation as shown by the $\kappa - \omega$ LSST model.

Interesting approaches for the enhancement of the turbulent kinetic energy have been proposed. A function for the boost of the production of turbulent kinetic energy has also been coupled to the transition $\kappa - \omega - \gamma$ SST model retrieving the beneficial effect of a transition function and, ensuring, at the same time, the enhancement of the friction levels.

VI. Ackowledgements

The work reported in this paper has been conducted in the GARTEUR AG59 project "IMoLA: Improving the Modelling of Laminar separation bubble" which includes the following members: CIRA, DLR, ONERA, Univ. of Napoli "Federico II", Imperial College, Marche Polithecnic University, Univ. of Southampton, Univ. of Strasbourg, Institute of Marine Engineering of National Research Council of Italy.

References

[1] Menter, F. R., Smirnov, P. E., Liu, T., and Avancha, R., "A One-Equation Local Correlation-Based Transition Model," *Flow, Turbulence and Combustion*, Vol. 95, No. 4, 2015, pp. 583–619. doi:10.1007/s10494-015-9622-4, URL `http://dx.doi.org/10.1007/s10494-015-9622-4`.

[2] Catalano, P., and Amato, M., "An evaluation of RANS turbulence modelling for aerodynamic applications," *Aerospace Science and Technology*, Vol. 7, No. 7, 2003, pp. 493–509.

[3] Catalano, P., Mele, B., and Tognaccini, R., "On the implementation of a turbulence model for low Reynolds number flows," *Computers and Fluids*, Vol. 109, 2015, pp. 67–71.

[4] Catalano, P., and de Rosa, D., "Large Eddy Simulations and RANS models for airfoils at low Reynolds number." *AIAA 2020 Aviation Forum*, 2020. AIAA paper 2020-2990.

[5] Bernardos, L., Richez, F., Gleize, V., and Gerolymos, G., "Prediction of Separation-Induced Transition on the SD7003 Airfoil Using Algebraic Transition Triggering," *AIAA Journal*, Vol. 57, No. 9, 2019. Https://doi.org/10.2514/1.J058288.

[6] De Santis, C., Catalano, P., and Tognaccini, R., "Model for Enhancing Turbulent Production in Laminar Separation Bubbles," *AIAA Journal*, Vol. 60, No. 1, 2022, pp. 473–487. doi:10.2514/1.j060883, URL `https://doi.org/10.2514/1.j060883`.

[7] Menter, F., Langtry, R., Likki, S., Suzen, Y., Huang, P., and Volker, S., "A correlation-based transition model using local variables - Part 1: Model formulation," *J Turbomach*, Vol. 128, No. 3, 2006, pp. 413–422.

[8] Medida, S., and Baeder, J., "Application of the Correlation–based γ–$\widetilde{\mathrm{Re}}_{\theta,t}$ transition model to the Spalart–Allmaras turbulence model," Honolulu, HI, 2011.

[9] Malan, P., Suluksna, K., and Juntasaro, E., "Calibrating γ–$\widetilde{\mathrm{Re}}_{\theta,t}$ Transition Model for Commercial CFD," *47th AIAA Aerospace Sciences Metting*, Orlando, FL, 2009.

[10] Spalart, P.R. and Allmaras, S.R., "A one-equation turbulent model for aerodynamic flows," *La Recherche Aérospatiale*, Vol. 1, 1994, pp. 5–21.

[11] Spalart, P. R. and Garbaruk, A. V., "Correction to the Spalart–Allmaras Turbulence Model, Providing More Accurate Skin Friction," *AIAA Journal*, Vol. 58, No. 5, 2020, pp. 1903–1905.

[12] Ilinca, F. and Pelletier, D., "Positivity preservation and adaptive solution of two-equation models of turbulence," *International Journal of Thermal Sciences*, Vol. 38, No. 7, 1999, pp. 560 – 571.

[13] Kang L. and Yue W. and Wen-Ping S. and Zhong-Hua H., "A two–equation local–correlation–based laminar–turbulent transition modeling scheme for external aerodynamics," *Aerospace Science and Technology*, Vol. 106, 2020, p. 106128.

[14] Baş, O., Ç. Çakmakçiŏglu, S., and Kaynak, U., "A Novel Intermittency Distribution Based Transition Model For Low-Re Number Airfoils," *31st AIAA Applied Aerodynamics Conference*, American Institute of Aeronautics and Astronautics (AIAA), 2013. doi:10.2514/6.2013-2531, URL `http://dx.doi.org/10.2514/6.2013-2531`.

[15] Del Álamo, J. C., and Jiménez, J., "Estimation of Turbulent Convection Velocities and Corrections to Taylor's Approximation," *Journal of Fluid Mechanics*, Vol. 640, 2009, pp. 5–26. doi:10.1017/S0022112009991029.

[16] Miozzi, M., Di Felice, F., Klein, C., and Costantini, M., "Taylor Hypothesis Applied to Direct Measurement of Skin Friction Using Data From Temperature Sensitive Paint," *Experimental Thermal and Fluid Science*, Vol. 110, 2020, p. 109913. doi:10.1016/j.expthermflusci.2019.109913.

[17] Eckelmann, H., "The Structure of the Viscous Sublayer and the Adjacent Wall Region in a Turbulent Channel Flow," *Journal of Fluid Mechanics*, Vol. 65, No. 3, 1974, pp. 439–459. doi:10.1017/S0022112074001479.

[18] Kim, J., and Hussain, F., "Propagation Velocity of Perturbations in Turbulent Channel Flow," *Physics of Fluids A*, Vol. 5, No. 3, 1993, pp. 695–706. doi:10.1063/1.858653.

[19] Hetsroni, G., Tiselj, I., Bergant, R., Mosyak, A., and Pogrebnyak, E., "Convection Velocity of Temperature Fluctuations in a Turbulent Flume," *Journal of Heat Transfer*, Vol. 126, No. 5, 2004, pp. 843–848. doi:10.1115/1.1797032.

[20] Liu, T., Sullivan, J. P., Asai, K., Klein, C., and Egami, Y., *Pressure and Temperature Sensitive Paints*, Springer International Publishing, Cham, 2021. doi:10.1007/978-3-030-68056-5_10.

[21] Ondrus, V., Meier, R., Klein, C., Henne, U., Schäferling, M., and Beifuss, U., "Europium 1,3-di(thienyl)propane-1,3-diones with Outstanding Properties for Temperature Sensing," *Sensors and Actuators A: Physical*, Vol. 233, 2015, pp. 434–441. doi:10.1016/j.sna.2015.07.023.

[22] Bitter, M., Hilfer, M., Schubert, T., Klein, C., and Niehuis, R., "An Ultra-Fast TSP on a CNT Heating Layer for Unsteady Temperature and Heat Flux Measurements in Subsonic Flows," *Sensors*, Vol. 22, No. 2, 2022. doi:10.3390/s22020657.

[23] Miozzi, M., Capone, A., Costantini, M., Fratto, L., Klein, C., and Di Felice, F., "Skin Friction and Coherent Structures Within a Laminar Separation Bubble," *Experiments in Fluids*, Vol. 60, 2019, p. 13. doi:10.1007/s00348-018-2651-8.

[24] Hoarau, Y., Pena, D., Vos, J. B., Charbonnier, D., Gehri, A., Braza, M., Deloze, T., and Laurendeau, E., "Recent Developments of the Navier Stokes Multi Block (NSMB) CFD solver," *54th AIAA Aerospace Sciences Meeting*, 2016. URL 10.2514/6.2016-2056.

[25] Vos, J. B., Charbonnier, D., Ludwig, T., Merazzi, S., Gehri, A., and Stephani, P., "Recent Developments on Fluid Structure Interaction Using the Navier Stokes Multi Block (NSMB) CFD Solver," *35th AIAA Applied Aerodynamics Conference*, American Institute of Aeronautics and Astronautics, 2017. doi:10.2514/6.2017-4458, URL https://doi.org/10.2514/6.2017-4458.

[26] Hoarau, Y., "Analyse physique par simulation numérique et modélisation des écoulements décollés instationnaires autour de surfaces portantes," Ph.D. thesis, Toulouse, France, 2002. URL http://theses.fr/2002INPT013H, thèse de doctorat dirigée par Braza, Marianna Dynamique des fluides.

[27] Marouf, A., "Analyse physique de concepts du morphing électroactif pour accroître les performances aérodynamiques des ailes du futur par simulation numérique de Haute Fidélité et modélisation de la Turbulence à nombre de Reynolds élevé," Ph.D. thesis, Université de Strasbourg, 2020. doi:https://www.theses.fr/s18407, URL https://www.theses.fr/s184078, thèse de doctorat dirigée par Hoarau, Yannick et Braza, Marianna, Mécanique Des Fluides.

[28] Bourguet, R., Braza, M., Harran, G., and Akoury, R. E., "Anisotropic Organised Eddy Simulation for the prediction of non-equilibrium turbulent flows around bodies," *Journal of Fluids and Structures*, Vol. 24, No. 8, 2008, pp. 1240–1251. URL https://doi.org/10.1016/j.jfluidstructs.2008.07.004.

[29] Marouf, A., Tekap, Y. B., Simiriotis, N., Tô, J.-B., Rouchon, J.-F., Hoarau, Y., and Braza, M., "Numerical investigation of frequency-amplitude effects of dynamic morphing for a high-lift configuration at high Reynolds number," *International Journal of Numerical Methods for Heat & Fluid Flow*, Vol. 31, No. 2, 2020, pp. 599–617. doi:10.1108/hff-07-2019-0559, URL https://doi.org/10.1108/hff-07-2019-0559.

[30] Donea, J., Giuliani, S., and Halleux, J., "An arbitrary lagrangian-eulerian finite element method for transient dynamic fluid-structure interactions," *Computer Methods in Applied Mechanics and Engineering*, Vol. 33, No. 1-3, 1982, pp. 689–723. URL https://doi.org/10.1016/0045-7825(82)90128-1.

[31] Spalart, P. R., and Allmaras, S. R., "A one equation turbulence model for aerodynamic flows," 30^{th} *AIAA Aerospace Sciences Meeting and Exhibit*, Reno, NV, 1992. AIAA paper 92-0439.

[32] Menter, F., "Zonal Two Equation k-w Turbulence Models For Aerodynamic Flows," *23rd Fluid Dynamics, Plasmadynamics, and Lasers Conference*, American Institute of Aeronautics and Astronautics, 1993. doi:10.2514/6.1993-2906, URL https://doi.org/10.2514/6.1993-2906.

[33] Cakmakcioglu, S. C., Bas, O., Mura, R., and Kaynak, U., "A Revised One-Equation Transitional Model for External Aerodynamics," *AIAA AVIATION 2020 FORUM*, American Institute of Aeronautics and Astronautics, 2020. doi:10.2514/6.2020-2706, URL https://doi.org/10.2514/6.2020-2706.

[34] Langtry, R., and Menter, F., "Transition Modeling for General CFD Applications in Aeronautics," *43rd AIAA Aerospace Sciences Meeting and Exhibit*, 2005. doi:10.2514/6.2005-522, URL http://dx.doi.org/10.2514/6.2005-522.

[35] Xiao, H., and Cinnella, P., "Quantification of model uncertainty in RANS simulations: A review," *Progress in Aerospace Sciences*, Vol. 108, 2019, pp. 1–31.

[36] Duraisamy, K., Iaccarino, G., and Xiao, H., "Turbulence modeling in the age of data," *Annual Review of Fluid Mechanics*, Vol. 51, 2019, pp. 357–377.

[37] Mishra, A. A., Mukhopadhaya, J., Iaccarino, G., and Alonso, J., "Uncertainty estimation module for turbulence model predictions in SU2," *AIAA Journal*, Vol. 57, No. 3, 2019, pp. 1066–1077.

[38] Iaccarino, G., Mishra, A. A., and Ghili, S., "Eigenspace perturbations for uncertainty estimation of single-point turbulence closures," *Physical Review Fluids*, Vol. 2, No. 2, 2017, p. 024605.

[39] Launder, B., Tselepidakis, D., and Younis, B., "A second-moment closure study of rotating channel flow," *Journal of Fluid Mechanics*, Vol. 183, 1987, pp. 63–75.

[40] Speziale, C. G., "On nonlinear kl and k-ε models of turbulence," *Journal of Fluid Mechanics*, Vol. 178, 1987, pp. 459–475.

[41] Emory, M., Larsson, J., and Iaccarino, G., "Modeling of structural uncertainties in Reynolds-averaged Navier-Stokes closures," *Physics of Fluids*, Vol. 25, No. 11, 2013, p. 110822.

[42] Banerjee, S., Krahl, R., Durst, F., and Zenger, C., "Presentation of anisotropy properties of turbulence, invariants versus eigenvalue approaches," *Journal of Turbulence*, , No. 8, 2007, p. N32.

[43] Horton, H. P., "Laminar Separation in two and three-dimensional incompressible flow," PhD thesis, University of London, 1968.

[44] Catalano, P., and Tognaccini, R., "Turbulence Modeling for Low-Reynolds-Number Flows," *AIAA Journal*, Vol. 48, No. 8, 2010, pp. 1673–1685. doi:10.2514/1.J050067, URL https://arc.aiaa.org/doi/abs/10.2514/1.J050067.

[45] Catalano, P., and Tognaccini, R., "RANS analysis of the low-Reynolds number flow around the SD7003 airfoil," *Aerospace Science and Technology*, Vol. 15, No. 8, 2011, pp. 615 – 626. doi:10.1016/j.ast.2010.12.006.

[46] Galbraith, M. C., and M. R. Visbal, "Implicit Large Eddy Simulation of Low Reynolds Number Flow past the SD 7003 Airfoil," 46^{th} *AIAA Aerospace Sciences Meeting and Exhibit*, 2008. AIAA paper 2008-225.

[47] Galbraith, M. C., and Visbal, M. R., "Implicit Large Eddy Simulation of Low-Reynolds-Number Transitional Flow Past the SD7003 Airfoil," *40th Fluid Dynamics Conference and Exhibit*, AIAA, Chicago, Illinois, USA, 2010. doi:10.2514/6.2010-4737.

[48] Catalano, P., and Tognaccini, R., "Numerical analysis of the flow around the SD7003 airfoil," 48^{th} *AIAA Aerospace Sciences Meeting*, 2010.

[49] Selig, M. S., Donovan, J. F., and Fraser, D. B., "Airfoils at Low Speeds," *Soartech 8*, H. A. Stokely, Soartech publications, Virginia Beach, VA, USA, 1989.

[50] Selig, M. S., Guglielmo, J. J., Groeren, A. P., and Giguere, P., "Summary of Low-Speed Airfoil Data," H. A. Stokely, Soartech Aero publications, Virginia Beach, VA, USA, 1995.

[51] McGhee, R., Walker, B., and Millard, B., "Experimental Results for Eppler 387 Airfoil at low Re numbers in Langley Low Turbulence pressure tunnel," Tech. Rep. TM 4062, NASA, 1988.

[52] Miozzi, M., Di Felice, F., Klein, C., and Costantini, M., "Taylor hypothesis applied to direct measurement of skin friction using data from Temperature Sensitive Paint," *Experimental Thermal and Fluid Science*, Vol. 110, 2020.

[53] Miozzi, M., Di Felice, F., Klein, C., and Costantini, M., "Taylor hypothesis applied to direct measurement of skin friction using data from Temperature Sensitive Paint," *Experimental Thermal and Fluid Science*, Vol. 110, 2020. Https://doi.org/10.1016/j.expthermflusci.2019.109913.

[54] Miozzi, M., Capone, A., Costantini, M., Fratto, C., L. Klein, and Di Felice, F., "Skin friction and coherent structures within a laminar separation bubble," *Experiments in Fluids*, Vol. 60, 2019. Https://doi.org/10.1007/s00348-018-2651-8.